

# Catalyst-coated slurry electrodes

Preparation, characterization and catalysis  
of silver nanoparticles on a carbon  
substrate for CO<sub>2</sub> reduction to CO

*Laura Bianca Donk*



# Catalyst-coated slurry electrodes

## Preparation, characterization and catalysis of silver nanoparticles on a carbon substrate for CO<sub>2</sub> reduction to CO

by

Laura Bianca Donk

to obtain the degree of Master of Science  
at the Delft University of Technology,  
to be defended publicly on Monday March 29, 2021 at 14:30.

Student number: 4468236  
Project duration: August 1, 2020 – March 29, 2021  
Thesis committee: Dr. ir. D. Vermaas, TU Delft, supervisor  
Dr. T.E. Burdyny, TU Delft  
Prof. dr. ir. J.T. Padding, TU Delft  
Daily supervision: N.E.G. Ligthart, TU Delft

An electronic version of this thesis is available at <http://repository.tudelft.nl/>.



# Preface

This document contains a detailed account of my thesis project under David Vermaas as a final fulfillment of the requirements for the degree of Master of Science. I study chemical engineering because I am passionate about finding solutions to enable the energy transition to renewable energy. This project matches with that, and idea of proving something new also fascinated me. Even though the proof for this concept is not there yet, I have enjoyed working on this project and value my personal growth during this time.

Firstly, I would like to thank David Vermaas for welcoming me in his group and providing helpful insights on both the experiments and their analysis. A special word of thanks to my daily supervisor, Nathalie Ligthart, who has been friendly and accommodating, provided constructive advice and taught me valuable research skills.

I also would like to thank Lorenz Baumgartner for teaching me how to set up a safe and functioning system for electrolysis, Andrey Goryachev for showing the art of impregnation and doing XPS/XRD measurements, Harrie Jansma for facilitating the use of a tube oven, Wiel Evers for the TEM images and Baukje Terpstra for the ICP-OES measurements. Additionally, I would like to extend my gratitude to all members of the Transport Phenomena group for their fun conversations and support during this process.

I would like to thank my friends and family who have provided all the mental support a thesis student could want, in the form of game nights, random 5 pm walks and stay-inns at 'hotel parents'. To end, a special mention to Sohan Phadke, who provided continuous support in the form of food, fun or feedback, whichever I needed.

*Laura Bianca Donk  
Delft, March 2021*



# Summary

Electrolyzers for CO<sub>2</sub> reduction can be used to synthesize renewable fuels, as a route to replace fossil fuels in our everyday economy with the purpose of minimizing the effects of climate change. For a high-scale implementation of electrolyzers, high operation current densities and low overpotentials are essential. Currently available options do not offer this and are limited by the low mass transfer of CO<sub>2</sub> in the system. We envision using catalyst-coated capacitive particles (slurry electrodes) to be a solution: a system where the reaction site can be brought to the reagent, instead of the other way around.

This thesis is a first step in the direction of a slurry electrode flow cell and aims to produce silver nanoparticles deposited on activated carbon particles to function as catalysts in such a system. The goal of the synthesis procedures was to produce a capacitive powder (activated carbon) with efficient deposition of silver nanoparticles (spheres) ranging 5-20 nm in diameter. Based on literature, the most interesting methods for synthesis were selected to be: solution-based methods with only activated carbon, with added polyvinylpyrrolidone, with added sucrose, electrodeposition and impregnation. The resulting powders were analyzed using ICP-OES and TEM, showing that only impregnation and electrodeposition can yield the desired powders with a near-100% silver deposition efficiency and particles < 20 nm in size.

Next, the impregnation and electrodeposition samples were prepared into a 15 wt% slurry, and a third slurry was made with bare AC as a blank. The catalysis experiments were executed in a flow cell (electrode area = 4 cm<sup>2</sup>), with currents ranging from -5 to -15 mA/cm<sup>2</sup>. Within this range of currents, extreme potentials up to -10 V (measured over working electrode versus counter electrode) were measured. The potentials on the anode and cathode side of the cell were also measured individually using reference electrodes, showing that the anodic side of the cell reached +5 V, whereas the cathodic side of this cell reached only -1 V. Additionally, CV scans before and after the experiments confirm that the cell's conductivity decreased within an experiment, however, this degradation is reversed for a new experiment. These observations combined lead us to believe that the cause of the cell problems is located on the anodic side of the system, and is most likely resistance from oxygen bubbles, which needs to be solved to allow cell operation at higher current densities.

Since the aim of the project was CO<sub>2</sub> reduction on the slurry electrodes, the outgoing gases from the cathode were measured in a GC. The blank was included to demonstrate the catalytic effect of the silver nanoparticles, yet the highest CO flow (around 0.05 ml/min) was measured at the lowest current density during this blank experiment. Calculating the Faradaic efficiency (FE) suggests that 33% of the electrons in that experiment was used for this conversion. The other measurements, at higher currents or with silver present, did not reach an FE of 10%. This combination leads to the conclusion that the observed CO is most likely not produced by CO<sub>2</sub> reduction. A hypothesis was made that this CO was already present at the powder's surface and released during the experiment, however XPS data showed that there were no noticeable differences in the content of oxygen-bound carbon between the coated samples and the bare sample. Thus, the source of the CO is at this stage unknown.

Future work towards proving CO<sub>2</sub> taking place on the slurry electrode should first investigate the source of the observed CO, which requires testing the influence of the different carbon sources present in the system. Additionally, the blank experiment should be improved: using a bare carbon slurry that underwent the same procedure as the coated slurry (without the precursor present) eliminates any differences in the powder.



# Glossary

**AC** Activated Carbon. 7, 10, 15, 16, 21, 22, 25, 32

**ALD** Atomic Layer Deposition. 9, 10

**CCS** Carbon Capture and Storage. 2

**CCU** Carbon Capture and Utilisation. 2

**CO<sub>2</sub>RR** CO<sub>2</sub> Reduction Reaction. 2, 7, 27, 31

**CV** Cyclic Voltammetry. 16, 17, 29, 30

**FE** Faradaic Efficiency. 3, 5, 32

**GC** Gas Chromatograph. 13, 17, 18, 31, 32

**GDE** Gas Diffusion Electrode. 2

**HER** Hydrogen Evolution Reaction. 5, 7, 31

**ICP-OES** Inductively Coupled Plasma Optical Emission Spectrometry. 11, 12, 18, 21, 22, 24

**OER** Oxygen Evolution Reaction. 2, 27

**PDA** Peripheral Differential Amplifier. 17, 27

**PVP** PolyVinylPyrrolidone. 7, 8, 10, 15, 16, 21–23, 25

**TEM** Transmission Electron Microscope. 11, 21–24

**XPS** X-ray Photoelectron Spectroscopy. 12, 21, 32



# Table of Contents

<b>1</b>	<b>Introduction</b>	<b>1</b>
1.1	The global need for CO <sub>2</sub> reduction	1
1.2	Economically feasible cell design for scaling up CO <sub>2</sub> reduction	2
1.3	This thesis: Catalyst development for CO <sub>2</sub> reduction on slurry electrodes	3
1.4	Research plan	3
1.4.1	Research objective	3
1.4.2	Research procedure	3
1.5	Report structure	4
<b>2</b>	<b>Theory and Literature</b>	<b>5</b>
2.1	Why and how: CO <sub>2</sub> reduction to CO	5
2.1.1	Why CO is selected as reaction product	5
2.1.2	Silver as a catalyst for CO <sub>2</sub> reduction to CO	5
2.2	Using nanoparticles for electro-catalysis	6
2.2.1	Synthesis: Nucleation and Growth	6
2.2.2	Silver nanoparticles for CO <sub>2</sub> reduction	7
2.3	Description and selection of synthesis methods	7
2.3.1	Wet syntheses	7
2.3.2	Gas phase syntheses	8
2.3.3	Method selection	10
2.4	Analysis techniques	11
2.4.1	Nanoparticle size: TEM	11
2.4.2	Silver deposition efficiency: ICP-OES	11
2.4.3	Oxidation state: XPS	12
2.4.4	Concentration of gaseous products: GC	13
<b>3</b>	<b>Experimental</b>	<b>15</b>
3.1	Materials	15
3.2	Synthesis of silver nanoparticles	15
3.2.1	Wet synthesis with reducing and/or stabilizing agents	15
3.2.2	Electrodeposition	16
3.2.3	Impregnation	17
3.3	Catalytic testing	17
3.4	Analysis methods	18
3.4.1	ICP-OES preparation	18
<b>4</b>	<b>Results and Discussion</b>	<b>21</b>
4.1	Synthesis of silver nanoparticles	21
4.1.1	Silver content	22
4.1.2	Particle size distribution	23
4.1.3	Stability of produced catalysts	24
4.1.4	Discussion on preferred synthesis method	25
4.2	Catalysis experiments	26
4.2.1	Flow cell electrochemistry	26
4.2.2	Reaction product analysis	31
<b>5</b>	<b>Conclusions and Recommendations</b>	<b>33</b>
5.1	Conclusions	33
5.1.1	Successful synthesis of nanoparticles	33
5.1.2	Poorly functioning anode	33
5.1.3	Questionable CO <sub>2</sub> reduction	33

---

5.2 Recommendations . . . . .	34
5.2.1 Nanoparticle deposition in final application . . . . .	34
5.2.2 Towards a proof of concept of the slurry electrode flow cell . . . . .	34
<b>Bibliography</b>	<b>35</b>
<b>Appendices</b>	<b>43</b>
<b>A Additional deposition data</b>	<b>43</b>
A.1 Silver oxidation state . . . . .	43
A.2 Particle size distribution . . . . .	44
<b>B Additional electrochemical data</b>	<b>45</b>
B.1 Impregnation . . . . .	45
B.2 Blank . . . . .	48
B.3 Electrodeposition . . . . .	51
B.4 CO <sub>2</sub> flow rate . . . . .	54

## Introduction

### 1.1. The global need for CO<sub>2</sub> reduction

Climate change, one of the consequences of the increased concentration of greenhouse gases in the atmosphere, has become a challenge of great importance in the 21<sup>st</sup> century. The effects of climate change include rising global temperatures, rising sea levels and the melting of glaciers, permafrost and polar ice caps. Scientific consensus has been reached that the cause of global warming is largely anthropogenic, related to the increased emission of CO<sub>2</sub> since the industrial revolution [1–6]. To illustrate this problem, Figure 1.1 shows the carbon cycle of the Earth, demonstrating fluxes and storage of carbon. Most fluxes are balanced, e.g. the carbon uptake from forests is approximately equally large as the carbon release out of forests (including soil). The main section where this balance is off, is the carbon release from industry (the main anthropogenic source of emission).

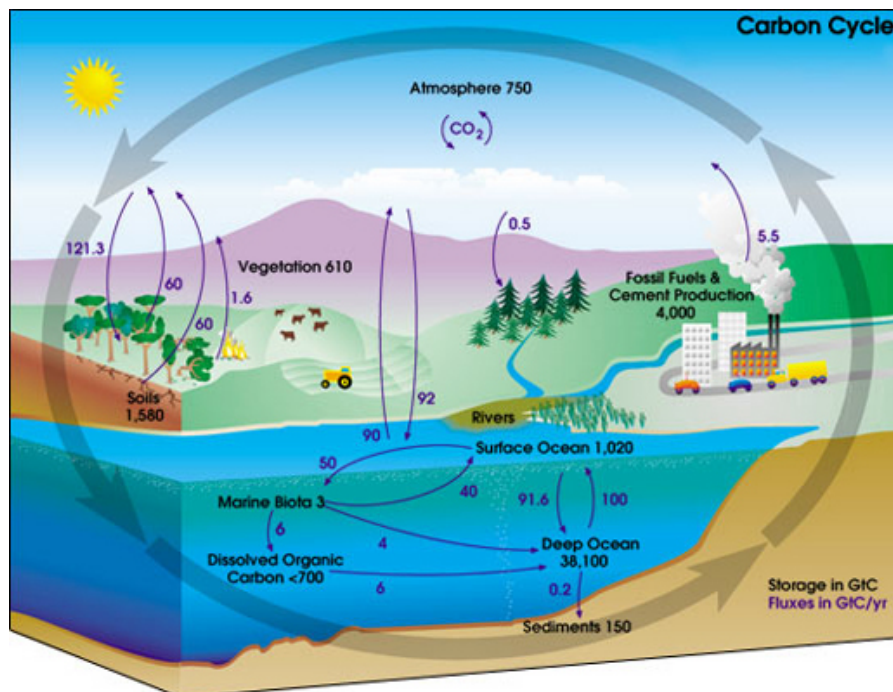


Figure 1.1: Artists' visualisation of the carbon cycle. Fluxes are shown in purple in Gt carbon/year, total amounts of stored carbon are shown in black. Note the high amount of carbon that is currently stored in fossil fuels and the high rate at which that is released into the atmosphere due to industrialisation. Source: NASA Earth Observatory [7]

To reduce the human impact on global warming, effort has been made to balance the human influence on the carbon cycle. A general consensus states that there are three main methods to accomplish this [8–10]:

- Reducing the carbon output of human industry, either by lowering the energy consumption or by use of more efficient technology.
- Utilizing the output of CO<sub>2</sub> for production of so-called carbon neutral feedstock and fuels, Carbon Capture and Utilisation (CCU) [11–13].
- Long-term storage of the CO<sub>2</sub> output in a closed environment, to prevent release into the atmosphere, so-called Carbon Capture and Storage (CCS) [14].

When combining CCU with the use of renewable energy, new possibilities emerge. If renewable energy is used to convert CO<sub>2</sub> to a feed stock or fuel, then a renewable fuel can be produced, thereby replacing fossil fuels. Renewable energy production is intermittent, and does not match the typical energy consumption pattern over a given short time period. Using excess renewable energy to produce a fuel will help the transition towards a circular economy [15, 16].

Conversion of CO<sub>2</sub> into fuels can be done by an electrolyzer, using renewable energy as the energy source. Electrolyzers use electricity to drive a non-spontaneous electrochemical reaction, such as conversion of CO<sub>2</sub> into CO. The electrochemical reduction of CO<sub>2</sub> takes place at the cathode, with the following half reaction:  $CO_2 + 2e^- + 2H^+ \rightleftharpoons CO + H_2O$ , also called the CO<sub>2</sub> Reduction Reaction (CO<sub>2</sub>RR). On the other side of the cell, the anode, generally oxygen is produced:  $2H_2O \rightleftharpoons O_2 + 4H^+ + 4e^-$ , also referred to as the Oxygen Evolution Reaction (OER). Combining these half reactions gives the following overall reaction:  $2CO_2 \rightleftharpoons 2CO + O_2$ . Each of these half reactions can occur at a certain potential, their thermodynamic reaction potential. Yet, the reactions also have energy barriers, which means that they would require an additional driving force for the reaction to occur. This driving force can be supplied in the form of an overpotential, provided by increasing the potential applied to the system beyond the reaction potential, however, this comes at the loss of energy efficiency. To circumvent this reduced energy efficiency, a catalyst can be used to bring the required overpotential down and increase the cell's efficiency. Among the more efficient catalysts for this reaction, silver nanoparticles are preferred for their low price to output ratio. More background on the reactions and catalysts will be discussed in Chapter 2.

## 1.2. Economically feasible cell design for scaling up CO<sub>2</sub> reduction

Different cell layouts are commonly used for CO<sub>2</sub> reduction, such as H-cells, flow cells and gas diffusion electrodes (GDE). In an H-cell, the simplest of these, two electrodes are connected by an electrolyte. Since the electrolyte is not mobile in this set-up, the mass transfer of CO<sub>2</sub> is regulated by diffusion and thus inherently slow. Additionally, the solubility of CO<sub>2</sub> in water is very low, such that the maximum attainable current density for CO<sub>2</sub> reduction in water is limited at approximately 30 mA/cm<sup>2</sup> [17]. The question is, what improvements need to be made in order to enable CO<sub>2</sub> reduction at a scale for implementation in a circular economy?

Kenis et al. developed a model to calculate the required performance of an electrolyzer to make an economically viable process. Their results show the need for high current densities of minimum 150 mA/cm<sup>2</sup>, catalyst durability (>3000 h), high selectivity (assumed 100% in their paper) and low overpotentials (achieved with good catalysts) to enable economically feasible processes [18].

In the meantime, research on improving cell configurations is geared around flow cells. In this set-up, the electrolyte is constantly flowed through the cell. The benefits of this are two-fold: firstly, a convective flow is generated, increasing mass transfer of CO<sub>2</sub> in the electrolyte. Secondly, reagents are supplied continuously and products are removed continuously, thus allowing for longer term operation and future industrial application.

To overcome the inherent problem of low solubility of CO<sub>2</sub> in water, efforts have been made to supply the CO<sub>2</sub> in gaseous form. In such cells, gas diffusion electrodes (GDE) are used, at which CO<sub>2</sub> in gaseous form reacts to form the desired products. Despite the promise of GDEs, they also have their own shortcomings, namely controlling gas and liquid pressures to prevent breakthroughs and the high cost of gas diffusion layers, which gets in the way of economic feasibility of a GDE based system [18].

## 1.3. This thesis: Catalyst development for CO<sub>2</sub> reduction on slurry electrodes

In this thesis, a different cell design will be studied: a slurry electrode flow cell. A slurry is a two-phase liquid, that consists of highly conductive and capacitive particles suspended in a solvent (usually in water). They can accept and pass on electrons, and in this way create a network of charged particles in the suspension. By introducing a catalyst on the surface of the slurry particles, electrochemical reactions will take place on the particles' surface instead of on the electrode (where the catalyst normally is), enabling use of a whole reactor compartment for the reaction.

The purpose of using a catalyst-coated slurry electrode is to create a more efficient and scaleable flow cell, allowing for higher currents and Faradaic efficiencies (FE). The hypothesis is that by bringing the catalyst to the reagent, instead of the other way around, the impact of CO<sub>2</sub> mass transport limitations can be reduced.

The use of slurries has gained attention in research for renewable energy storage. Most research with slurries is focused on electrochemical flow systems, allowing large amounts of charge to be stored in a reservoir of particles, similar to a flow battery [19–24]. The use of slurry electrodes is building on that principle.

Figure 1.2 shows a visual comparison of different cell architectures, comparing the slurry flow cell as described here to more established cell architectures, the H-cell and the regular flow cell, described in the previous section. The main challenge in the slurry electrode flow cell are assumed to lie in the production and stability of a suitable catalyst deposited on the particles, hence producing and testing the catalyst-coated particles is the focus of this thesis.

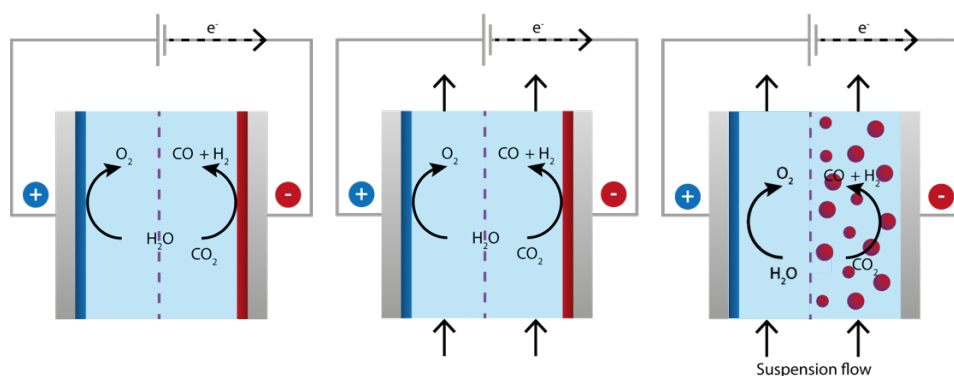


Figure 1.2: From left to right: H-cell, flow cell, slurry flow cell. In an H-cell, the electrolyte is stagnant. In a flow cell, the electrolyte with reagents is constantly flowed through the cell. The reactions take place at the plate electrodes. In the slurry flow cell, capacitive microparticles coated with a catalyst have been added to the electrolyte. The reaction takes place at their surface, and plate electrodes have been replaced by current collectors. Image adapted from Nathalie Lighthart [25].

## 1.4. Research plan

### 1.4.1. Research objective

The aim of this thesis is to find a practical method to create a working catalyst coated slurry to use for CO<sub>2</sub> reduction in a slurry electrode flow cell. The research consists of two parts, centered around the following research questions.

*'Which of the tested deposition methods yields a powder with a highly efficient and stable silver loading, and small spherical silver nanoparticles (5-20 nm)?'*

*'Which of the tested deposition methods for making the catalyst-coated slurry results in the lowest overpotential and highest Faradaic efficiency when used in a CO<sub>2</sub> reduction slurry electrode flow cell?'*

### 1.4.2. Research procedure

In the process of answering the questions posed in the previous section, three phases can be distinguished: a literature study, experiments in which synthesis methods are used to make silver-coated

capacitive particles, and experiments in which those are used as slurry electrodes in a flow cell for CO<sub>2</sub> reduction. In the first phase, a wider range of possible methods is investigated in a literature study, screening their possible advantages and disadvantages for this application. The most advantageous methods are selected for trials in the laboratory and subsequent analysis. Synthesised samples that fit the requirements of the first research question are produced in larger batch to be used for CO<sub>2</sub> reduction in a flow cell. These experiments then give information on the catalytic performance of the catalyst coated slurry.

## **1.5. Report structure**

This introduction provided the reader with a motivation for the research, the research objective and central hypothesis. Chapter 2 provides a fellow student reader with relevant background information to this project and includes information on the selection process for different synthesis methods. Chapter 3 describes how all experimental work is executed. Chapter 4 describes and discusses the obtained results. Section 4.1 provides insight into the syntheses performed, whereas Section 4.2 examines the results of the catalysis experiments. Chapter 5 concludes the work, and provides recommendations for future improvements.

# 2

## Theory and Literature

### 2.1. Why and how: CO<sub>2</sub> reduction to CO

#### 2.1.1. Why CO is selected as reaction product

Electrochemical CO<sub>2</sub> reduction is possible with different products in mind. A selection of common reaction products and properties of the reaction is shown in Table 2.1. One should notice that all the reaction equilibrium potentials ( $E^0$ ) are very close to 0 V versus Reversible Hydrogen Electrode (RHE), which is the potential at which H<sub>2</sub> is formed (the hydrogen evolution reaction, HER). Thus, all reactions are competing with the HER and a good catalyst provides a high Faradaic efficiency (FE, fraction of electrons going to a certain product) for the selected product.

Table 2.1: Main products of electrochemical CO<sub>2</sub> reduction, the amount of electrons involved in proton coupled electron transfers ( $n$ ), their equilibrium reduction potentials ( $E^0$ ) and market estimations.

Product	$n$	$E^0$ (V versus RHE) [26]	Market price (USD/tonne) [27]	Market size (Mtonne/year) [27]
Carbon monoxide (CO)	2	-0.10	236	150
Formic acid (HCOOH)	2	0.04 (pH 8)	225-332	1.02
Methanol (CH <sub>3</sub> OH)	6	0.02	174-235	98.9
Ethylene (C <sub>2</sub> H <sub>4</sub> )	6	0.08	474-609	184

This research is focused on CO as reaction product, for several reasons. First and foremost, there is a reasonable demand for CO, mostly used in the form of syngas (CO + H<sub>2</sub>) as a feedstock for the Fischer-Tropsch process. The Fischer-Tropsch process converts syngas to various liquid hydrocarbons (fuels) and is industrially executed, allowing for scalability [17, 28].

Additionally, the reaction to form CO only requires the transfer of two electrons ( $n=2$ ). For two-electron transfer reactions, there is typically only one intermediate, making it more simple to find an optimum catalyst. The synthesis of products that require more electron-transfers is kinetically challenging, as it requires a large overpotential with currently available catalysts [17, 26].

Lastly, the market price for CO is reasonably high compared to the other products, making economic feasibility more easily achieved. For more complex hydrocarbon products, the market price is possibly higher, but they are currently produced at very low costs with conventional industrial processes. It is hard to compete with those for electrolysis [17].

#### 2.1.2. Silver as a catalyst for CO<sub>2</sub> reduction to CO

Common catalysts with a high selectivity towards CO are generally monometallics. Hori et al. studied the selectivity of metal electrodes for CO in 1993 and derived a series from their results [29]. They found Au, Ag, Cu and Zn to be the most selective (in that order) and these are still commonly used catalysts to date. A more recent review by Jones et al. still refers to Au and Ag as the catalysts of choice for CO production [28]. They catalyze the reaction to proceed at relatively smaller overpotentials and higher current densities than many other catalysts. Between the choice of gold and silver, gold is generally the

better catalyst whereas silver is more affordable and available. Particularly because of this last aspect's importance for scalability of future applications, silver was chosen as the catalyst for this project. In the same paper, nanoparticles are identified as a research field of interest. This topic will be discussed later in the next section. More information on the fundamentals of electrochemical CO<sub>2</sub> reduction reactions can be found in Chapter 8 of *Modern Aspects of Electrochemistry*, written by Y. Hori [30].

## 2.2. Using nanoparticles for electro-catalysis

### 2.2.1. Synthesis: Nucleation and Growth

#### Formation of crystals

Chemical nanoparticle synthesis is usually done via a bottom-up method: assembly of particles from smaller fragments, e.g. atoms. Nucleation, the transition from atoms in solution to combined particles, plays a large role in such methods. The main theory on nucleation applies equilibrium thermodynamics and is based on the classical nucleation theory, which was developed by Becker and Döring in the 1930s [31]. Its basis lies in transition systems (condensation of vapor) minimizing their Gibbs free energy and it forms the basis for LaMer's theory about crystallization of solids [32].

Solutions with such smaller fragments present can be expressed as a dynamic equilibrium. For the formation of silver nanoparticles, the relevant equilibrium equation is:  $Ag^+ + e^- \rightleftharpoons Ag(s)$ . Crystals form above the equilibrium concentration, a condition which is called supersaturation. Supersaturation is when the chemical potential of the monomers in the crystal is lower than of the monomers in solution, and thus is the driving force for crystallization. Nevertheless, crystal formation is not thermodynamically favorable, since the small crystals at formation have a very high surface to volume ratio and thus a large amount of surface tension, a driving force pushing to solution of the particles.

Combining these two factors, the Gibbs free energy for nuclei contains a positive and a negative term. Figure 2.1 shows both the free energy for bulk and surfaces and the combined curve for the free energy of nuclei. This nuclei free energy has a maximum at radius  $r_c$ , the critical radius. At this point, the corresponding energy barrier is called the activation energy,  $\Delta G_c$ . For nuclei smaller than  $r_c$ , growth leads to an increase in the free energy, thus is unfavorable, and dissolution becomes more probable. For nuclei larger than  $r_c$ , growth leads to a decrease in free energy, and is thus favored.

The explanation above covers homogeneous nucleation. Heterogeneous nucleation differs from this, in the essence that there is a site or surface available at which nucleation can occur. The assumption of heterogeneous nucleation is that the presence of such sites decreases the activation energy barrier and thus makes nucleation at these sites more preferable.

#### LaMer: separation of nucleation and growth

The LaMer model (based on his original paper from 1950 [34]) describes nucleation and growth taking place separately, which assumes no new nuclei are formed during the growth phase. This assumption is based on the fact that the initial particle formation takes place in shorter time frame than the growth mechanisms. This situation is obtained when there is rapid nucleation above the supersaturation concentration. Before growth mechanisms take place, the formation of nuclei has lowered the monomer concentration below the supersaturation concentration again and nucleation has stopped. In this situation, the particle concentration increases rapidly during nucleation and stays more or less constant during the growth phase. As a consequence: to make many small particles, very rapid nucleation is needed. When nucleation is slower, the result is fewer, larger particles [33].

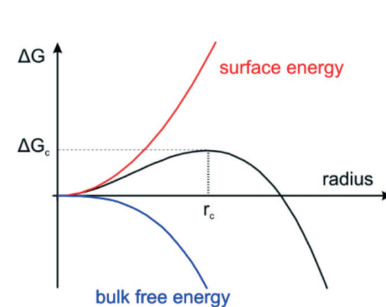


Figure 2.1: Gibbs free energy diagram comparing free energy for bulk (blue) and surface (red) processes. In black, the free energy for crystal formation is shown as the combination of bulk and surface.  $R_c$  is the critical nucleus size. Image reproduced from: Polte et al. [33].

### 2.2.2. Silver nanoparticles for CO<sub>2</sub> reduction

Catalysts are used to lower the activation energy for a chemical reaction and thus lower the energetic threshold for a reaction to take place. Nanoparticles gained attention for their high catalytic activity, compared to bulk material. For example, Salehi-Khojin et al. conducted a study on the effects of the size of spherical silver nanoparticles on their catalytic properties. Their study shows the highest CO production for particles of 5 nm in size and still a four-fold increase in activity for 40 nm particles compared to bulk silver, as can be seen in Figure 2.2 [35]. In this thesis, these results formed a target for size properties in the synthesis of nanoparticle catalysts.

In the process of understanding this size-based catalytic activity, studies such as the one by Back et al., have modeled the active sites of silver and gold nanoparticles, illustrating that differently coordinated sites (facets, corners, edges) have a different stabilizing effect on reaction intermediates, for both the CO<sub>2</sub>RR and HER reactions [36]. Since the relative presence of these sites depends on the nanoparticle size, the existence of an optimum is explained.

The review paper by Mahyoub et al. explains more extensively why factors such as size, morphology and porosity, all commonly mentioned as a reason for nanoparticles' increased catalytic activity, have an effect on the catalytic properties of silver nanoparticles for CO<sub>2</sub> reduction [37].

The remaining question is how many of those silver nanoparticles are needed to assure they are not the limiting factor in this system. Previous studies report their silver quantity as a mass per area of electrode (e.g. 0.1 mg/cm<sup>2</sup> in [38] and 5 mg/cm<sup>2</sup> in [35], both GDEs). However, this measure is not necessarily to be compared directly to the quantity of silver on the slurry electrode. If a direct comparison is made, a loading of 5 mg/cm<sup>2</sup> is equal to 0.2 wt% Ag (based on 15 wt% slurry, density 1100 kg/m<sup>3</sup>). At this stage, a loading of 4 wt% was aimed for, on the basis that it is better to be on the high end, to assure the silver content is not limiting for catalysis. At a later stage it could be worth investigating the ideal loading.

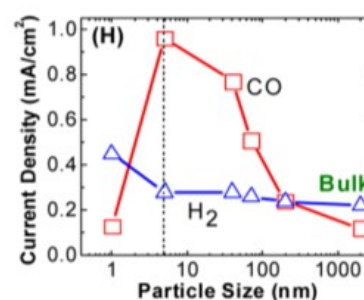


Figure 2.2: Current density for CO and H<sub>2</sub> production as a function of particle size. Measured at -0.75 V vs SHE (Standard Hydrogen Electrode). The maximum CO production occurs at a particle size of 5 nm. Image reproduced from: Salehi-Khojin et al. [35].

## 2.3. Description and selection of synthesis methods

This section provides an overview of possible synthesis methods to yield silver nanoparticles on a carbon powder substrate. These bottom-up methods to synthesize silver nanoparticles often work with a precursor, AgNO<sub>3</sub>, and a reductant. This section does not include all possible options, only common ones that are deemed relevant for this project. In section 2.3.3, a selection of the most promising methods that are included in the laboratory experiments is motivated.

### 2.3.1. Wet syntheses

#### Wet synthesis with reductants and stabilizers

In general, these solution based syntheses are performed via a hot injection method. Hot injection synthesis rapidly creates a very high supersaturation and fast nucleation due to the high temperature, and thus results in smaller particles, following LaMer's theory. Firstly, the reductants (and stabilizing agents) are dissolved in water and heated, usually to the boiling point of the mixture. Then, a precursor solution is injected rapidly and the system is left to react. To stop the reaction, the heating source is removed. These steps are visualized in Figure 2.3. Stabilizers are generally added to lower the barrier for nucleation in solution and to prevent particle aggregation. Four different categories can be identified within this section: syntheses based on presence of AC alone, syntheses with additional stabilizers present, syntheses with strong reductants present, and syntheses relying on the combination of both.

Based on these categories, several syntheses can be interesting to deposit silver nanoparticles on the carbon powder. Carbon powder has been identified as a weak reductant in earlier studies [40]. Therefore, a very simple synthesis method could involve the carbon powder and the silver precursor only. In this way, all reacting silver is already close to the carbon particles, which can be beneficial in terms of deposition on those particles.

A second method could include a stabilizing agent, for example polyvinylpyrrolidone (PVP), which is

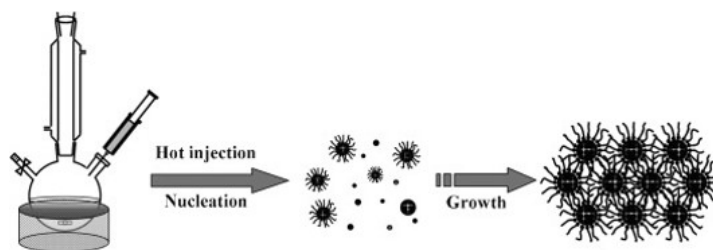


Figure 2.3: Schematic overview of hot injection nucleation, where nucleation and growth processes play a significant role. Image reproduced from: Park et al. [39].

previously identified to form a complex with silver that promotes nucleation [41]. Compared to the synthesis without PVP, this synthesis will probably allow for better control of the formation of the particles, although their formation in solution is also stabilized, which might result in a lower deposition.

Another synthesis option could be to use a strong reductant, such as sodium borohydrate, to promote rapid nucleation to yield small particles. In this synthesis, the ions present in solution for reduction, also help stabilizing the formed nanoparticles against aggregation [42]. This creates an electrostatic double layer around the nanoparticles, which repels them from each other, but would also repel them from the apolar carbon substrate. Despite this synthesis' high control over particle size, this can come at the cost of low deposition.

Lastly, the attention was drawn to a paper by Filippo Manno et al. that describes a green synthesis of silver nanoparticles, using sucrose as the reductant and stabilizer [43]. This synthesis relies on heat to split sucrose into glucose and fructose, which then act as reducing and stabilizing agents. The benefit of this synthesis is again a good control over particle size and since the stabilizing agents here are less charged than ions in solution, deposition becomes more likely.

### Electrodeposition

Electrodeposition, where the precursor is reduced electrochemically, is usually done on a solid support, which in the set-up is also the cathode [40]. For a visualization of the standard set-up, refer to Figure 2.4. Performing electrodeposition on a powder is more complex: it would involve making a current collector that passes on the charge to the carbon particles, where silver is then deposited. In order to have a high deposition efficiency with this method, it is important to minimize silver deposition on the current collector, which could be achieved by using a mesh.

Nevertheless, electrodeposition is a common method to deposit silver nanoparticles and allows for control over particle growth, for example by varying the applied potential [44], and particle shape, for instance by using additives [44], although this is out of scope for this thesis.

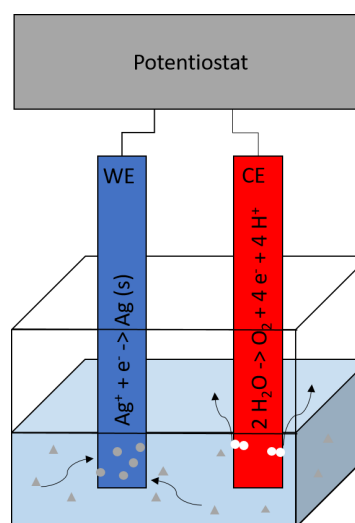


Figure 2.4: Schematic visualization of a standard electrodeposition set-up with two electrodes. The cathodic reaction takes place at working electrode (WE), e.g. silver deposition, the anodic reaction at the counter electrode (CE), such as oxygen evolution.

### 2.3.2. Gas phase syntheses

Gas phase syntheses, such as impregnation and atomic layer deposition, have been pointed out to be more scaleable and viable as industrial processes for nanoparticle synthesis [45]. They can be more complex to execute but offer accurate deposition in return.

### Impregnation

Impregnation is a mix between liquid and gas phase syntheses, where the solid support is brought into contact with a precursor solution first, which is then evaporated and the deposited salt is consequently reduced to nanoparticles under a reducing gas flow, as seen in Figure 2.5. It is a very suitable method to synthesize nanoparticles on porous substrates, like the carbon powder. Incipient wetness impregnation is a slightly modified method, where only a small solvent volume is used, that maximum fills the pore volume. In this way, capillary forces pull the solution inside, assuring deposition inside the pores. This is less suitable for a synthesis with carbon powder and water, as the powder is quite hydrophobic and thus capillary action will result in the opposite [46].

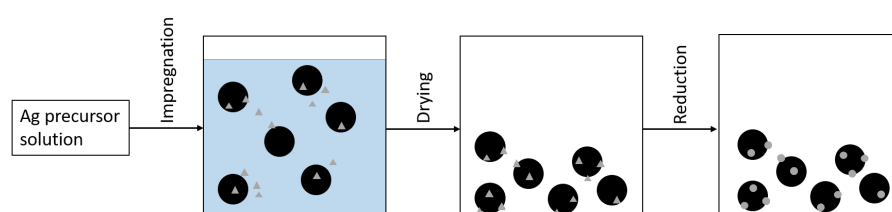


Figure 2.5: Schematic representation of the steps involved in impregnation synthesis. The larger black circles represent the carbon particles, the gray triangles represent the silver salt and the gray circles represent silver nanoparticles.

Impregnation is a method that allows for accurate control over the quantity of silver deposited, although very high concentrations are not possible, as high supersaturation can lead to premature crystal formation. Impregnation is a method commonly used to synthesize catalysts in industry [46] and is thus very suitable for scaling up at later stages. Nevertheless, it is also known as a method that can result in particles that are distributed heterogeneously in terms of locations [47]. Especially drying conditions are known to have a large influence on the resulting particles and this is also the main factor that can be altered to change the particle's spatial distribution [48].

### Atomic layer deposition

Atomic layer deposition (ALD) is a deposition technique that allows for accurate control over the amount of material deposited. The technique relies on the separation of the deposition reaction into two different, self-limiting steps. For each reaction, chemisorption takes place as a monolayer and then the sample is purged, to remove any non-absorbed material [45, 49, 50]. Figure 2.6 shows a schematic representation of these, usually two, sequential steps.

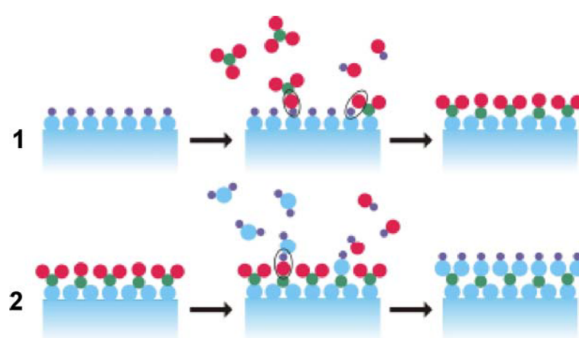


Figure 2.6: Schematic representation of the sequential reactions as used for ALD. 1. Chemisorption of the precursor, in this example tri-methyl-aluminium, on the substrate surface. 2. Reaction of the precursor with the second reactant, in this example water. In between the steps, purging takes place to prevent unwanted side-reactions. Image reproduced from: Van Ommen et al. [45].

ALD is commonly used to synthesize metal nanoparticles, however, preparing silver (and gold) particles using ALD is rather complex [51, 52]. In the set-up available for ALD, it is not possible to do ALD with a silver precursor, as it requires a special pre-treatment.

### 2.3.3. Method selection

In order to make a selection of which of the methods above most sensible to synthesize in laboratory, a Pugh matrix was used. A Pugh matrix is a helpful tool for making design choices, where a number of criteria important to the design are selected and given a weight based on their importance. Then, the base design option scores a 0 on all of the criteria and the other options are scored relatively to that with scores ranging -2 to 2, for example. Then, weighted scores are calculated to give a better assessment of the options.

In this project, executability is of highest importance, as the project timeline is rather short and some options might not be feasible to execute within that timeline. Next, the deposition efficiency of silver on the carbon substrate is given high importance too. This criterion does not only refer to the ability of the method to produce nanoparticles, but also whether the method leads to deposition on the carbon substrate, as not all methods inherently promote this.

Controllable particle size, scalability for future applications and opportunities for alteration, e.g. by changing concentrations or additives, are also included in the analysis. Generally, a method scores a 0 when it has no added benefits or downsides compared to the chosen base-case: solution synthesis with only activated carbon powder present. A score of -1 means that there is one downside, -2 means there are several, similarly for positive scores: a score of +1 means one benefit and a score of +2 means multiple benefits.

The Pugh matrix for the selection of the most suitable methods for synthesis in this project is shown in Table 2.2. The scores are based on the explanations given in the previous sections. As seen in the table, syntheses with a strong reductant present are considered less suitable for this project. The low score is caused by the expected lower deposition on the carbon substrate. Both the synthesis with only AC present or with added PVP score equally a 0, ALD and the synthesis with sucrose score higher with a 5 and a 3, respectively. The highest scores are given to synthesis methods impregnation and electrodeposition.

Table 2.2: Pugh matrix for method selection. 1. AC only, 2. PVP, 3. strong reductant, 4. Sucrose, 5. Electrodeposition, 6. Impregnation, 7. ALD.

Criteria	Weight	1	2	3	4	5	6	7
High deposition efficiency	4	0	-1	-2	-1	1	1	1
Controllable nanoparticle size	3	0	1	1	2	1	0	1
Opportunities for further alteration	1	0	1	1	1	2	1	1
Executable within project timeline	5	0	0	0	0	0	0	-1
Scaleability for future applications	2	0	0	0	0	1	1	1
Total +		0	4	4	7	11	7	10
Total -		0	-4	-8	-4	0	0	-5
Weighted score		0	0	-4	3	11	7	5

Since these scores are based on certain assumptions, it is important not to make too strict selections at this stage. Also, some methods are very similarly executed and can thus all be investigated without too much extra laboratory work. Therefore, all synthesis methods that score a zero or higher were included in the synthesis phase, except for ALD, as it is not possible to execute within the project timeline. The synthesis method using a strong reductant is kept in mind in case the other methods turn out to be unsatisfactory in producing particles of the right size.

## 2.4. Analysis techniques

This section includes a description of the analysis techniques used in this thesis and what they are used for. It is included to provide the reader with an understanding of how the technique works, allowing for better understanding of how the results were obtained.

### 2.4.1. Nanoparticle size: TEM

A transmission electron microscope (TEM) is an electron microscope that uses a high-voltage beam to illuminate a sample and create an image. In this thesis, the TEM was used to visualize the produced silver nanoparticles on their carbon substrate. These images were further processed to determine the particle size distribution per synthesis method.

Figure 2.7 shows a schematic overview of a TEM and its main components. The electron gun provides electrons, which are then accelerated and focused on the sample using electromagnetic lenses. The electrons then reach the sample. Samples have regions that are either transparent for electrons, in which case the beam is transmitted, or regions that are not transparent for electrons, in which case the beam is (partially) scattered. Either way, the TEM produces an image of how electrons interact with the sample. The resulting image is magnified by the lenses of the microscope. To view this image, it can be projected on a fluorescent viewing screen, it can be recorded by photographic film or it can be coupled to a sensor. The last of these allows for connection to a computer [53, 54].

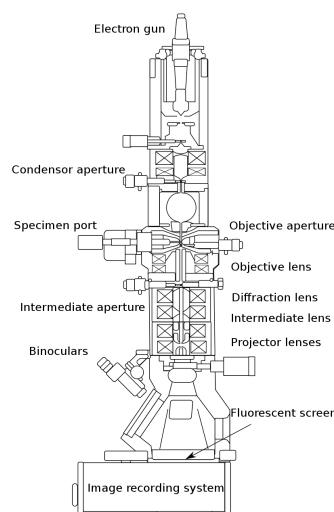


Figure 2.7: Schematic visualization of TEM system and its main components. Image reproduced from: Wikipedia [53].

### 2.4.2. Silver deposition efficiency: ICP-OES

Inductively coupled plasma optical emission spectrometry (ICP-OES) is an analysis technique that is commonly used to determine chemical composition and concentration of samples. In this thesis, ICP-OES was used to determine the silver content of the produced catalysts.

In ICP-OES, the emission spectrum of a component is used to determine its quantity in the sample. Figure 2.8 shows an overview of all the elements involved in ICP-OES. Firstly, the solution is pumped through a nebulizer to produce an aerosol, which is then led into a plasma (ionized gas, usually Argon, prepared by a strong electric field). Directly when the sample is loaded into the torch, it comes into contact with the extremely hot plasma (7000 K). As a result, the sample is destructed by ionization. Because of the high temperature, the electrons reach a higher, excited, state. When the electrons leave the torch and cool down, they drop back to their ground energy level and release their energy in photons. The photons are then measured in the spectrometer to determine the contents of the sample, as each element has its own typical emission spectrum. [55, 56].

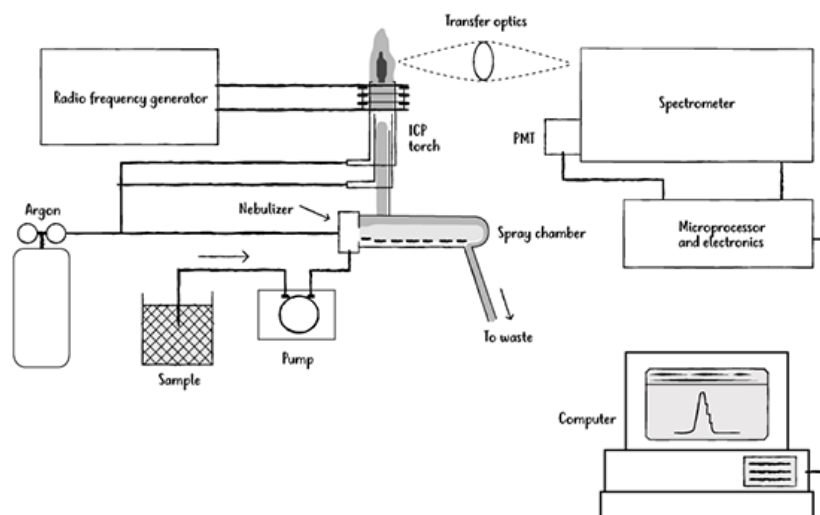


Figure 2.8: Visualization of ICP-OES system. On the left, the elements involved with both sample treatment to aerosol and plasma formation are shown. On the right, the spectrometer detects the sample's emission spectrum and this is further processed on a computer. Image reproduced from: Mindy Levine [56].

### 2.4.3. Oxidation state: XPS

X-ray photoelectron spectroscopy (XPS) is a spectroscopic technique which allows for quantitative analysis of a surface. It can measure the elemental composition and the elements' chemical state (oxidation state) at the sample's surface. What makes XPS powerful, is that it not only shows what elements are present, but also what other elements they are bonded to, which allows for more precise understanding of the chemical structure of the examined sample. In this thesis, XPS is used to analyse the oxidation state of both silver and carbon at the samples' surface.

In XPS, a sample is irradiated with X-rays and the resulting photoemission spectrum is measured. Described by the photoelectric effect, electrons ejected are measurable as a photon with the kinetic energy of exactly the difference between the energy of irradiation and the energy needed to remove the electron from the atom. In such way, the kinetic energy and quantity of ejected electrons determine which material they are from and the quantity of its presence [57–59].

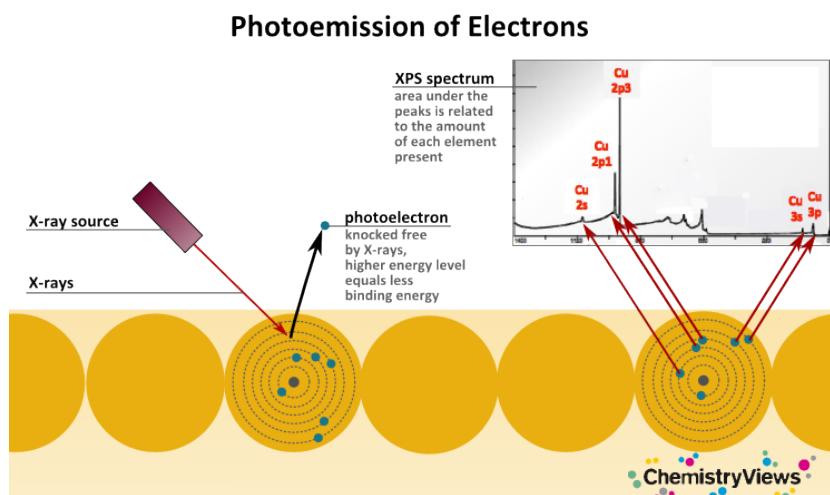


Figure 2.9: Visualization of how XPS measures the elemental state by making use of the photoelectric effect. Image reproduced from: ChemViews Magazine [57].

### 2.4.4. Concentration of gaseous products: GC

Gas chromatography (GC) is a quantitative analytical technique that is used to determine the composition of gaseous samples. In this thesis, GC is used to analyse the gases produced on the cathode side of the flow cell. Particularly, the presence and quantity of CO, CO<sub>2</sub> and H<sub>2</sub> were measured and then used to calculate the Faradaic efficiency of the reaction.

Similar to other chromatography techniques, GC uses a stationary and a mobile phase to separate different compounds. In GC, the mobile phase is an inert carrier gas, and the stationary phase is normally a liquid or polymer on a solid support. GC separates the gases due to their different affinity for the stationary phase, leading to different retention times for different compounds. Figure 2.10 displays a schematic visualization of the different elements in a gas chromatograph. A sample is injected into the stream of carrier gas and then carried into an oven, where the temperature is high enough to assure all components are in the gaseous phase, without decomposing them. Then, the sample reaches the column with the stationary phase and separation of compounds takes place, owing to gases' differing affinities for the stationary phase and their differing volatilities. Lastly, the individual components reaches the detector at different times, their elution time [60–62].

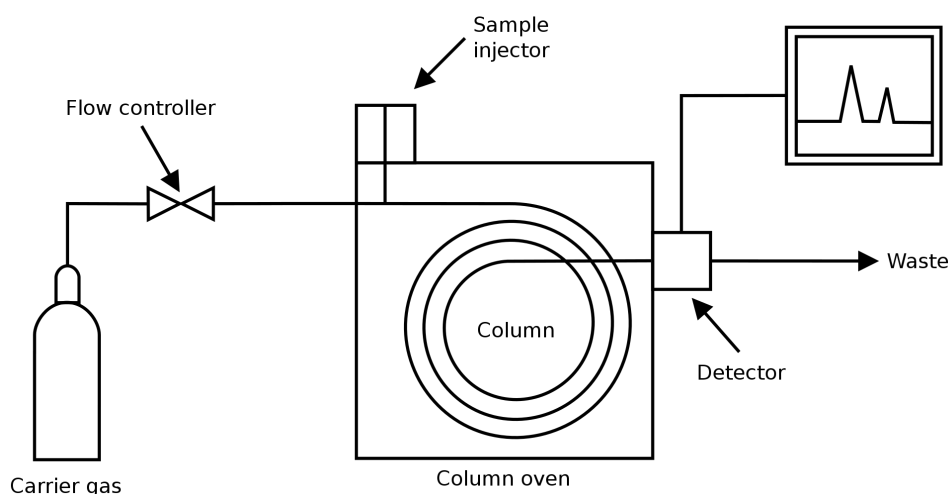


Figure 2.10: Visualization of GCsystem. Image reproduced from: Wikipedia [60]

In order to analyze the data from the detector, a gas chromatograph is normally calibrated with samples of known concentration. This confirms the retention time for a certain compound and the peak area for a certain concentration. Figure 2.11 shows an example chromatogram from one of the experiments. As seen, individual gases are identified by comparing their elution time to the compound's retention time. To determine the quantity present, the surface area of the peak with respect to the baseline is measured. In orange, one peak is colored to show the area described.

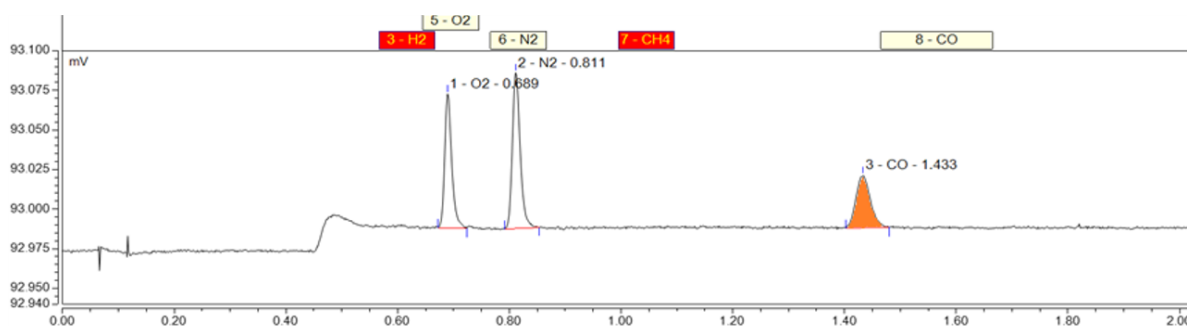


Figure 2.11: Example of GCresults, showing the peak locations in comparison to the calibrated retention times (shown on top). One peak is colored orange, showing the surface area used to determine the concentration.



# 3

## Experimental

### 3.1. Materials

The different chemicals used for the experimental work are listed in Table 3.1.

Table 3.1: Materials used for the experimental work in this thesis, including information on purity and supplier.

Chemical & Formula	Grade/info	Supplier
Nitric acid (HNO <sub>3</sub> )	99.9999 % pure, metals basis.	Alfa Aesar
Norit SX Plus Cat (Activated carbon, AC) (C)	65-70% solution in water median diameter = 20 μm	Aldrich
Polyvinylpyrrolidone (PVP) ((C <sub>6</sub> H <sub>9</sub> NO) <sub>n</sub> )	M <sub>w</sub> = 40,000	Alfa Aesar
Silver nitrate (AgNO <sub>3</sub> )	Premion, 99.9995% metals basis	Alfa Aesar
Potassium bicarbonate (KHCO <sub>3</sub> )	BioUltra, ≥99.5%	Sigma-Aldrich
Potassium hydroxide (KOH)	50% w/v in water	Alfa Aesar
Potassium nitrate (KNO <sub>3</sub> )	99%	Alfa Aesar
Sucrose (C <sub>12</sub> H <sub>22</sub> O <sub>11</sub> )	-	J.T. Baker

### 3.2. Synthesis of silver nanoparticles

#### 3.2.1. Wet synthesis with reducing and/or stabilizing agents

##### AC as only reductant

This synthesis was selected on the basis that activated carbon has been identified as a weak reductant in previous research [40]. In a typical synthesis for a 4 wt% loading, 0.5 g AC was suspended in 100 ml demiwater in a 3-neck round bottom flask and sonicated for 15 minutes. The suspension was then connected to a reflux tube and heated with a heating clamp under stirring until boiling. Next, 2.5 ml of a 0.039 M silver nitrate solution was injected rapidly. After 30 minutes of stirring, the heating source was removed and the solution was left to cool down. Afterwards, the silver coated particles were separated from the reaction solution using vacuum filtration over a Buchner funnel. The filter paper (Whatman 602 H 1/2) was pre-rinsed with 30 ml demiwater, then the suspension was filtered and the resulting powder was washed three times with approximately 30 ml demiwater. The powder was dried in an oven for 2 hours at 120 °C and afterwards stored in a dark cabinet.

##### Sucrose as reductant/stabilizing agent

This research procedure is an adaptation based on the work by Filippo et al. [43]. In a typical synthesis for a 4 wt% loading, 5.0 g of sucrose was dissolved in 100 ml water in a 3-neck round bottom flask and connected to a reflux tube. The solution was heated under stirring to its boiling point. Next, 2.5 ml of a 0.039 M silver nitrate solution was injected rapidly. After 30 minutes of stirring, the heating source

was removed and the solution was left to cool down. To incorporate deposition on AC, two different variations were executed.

For the two-step synthesis, based on homogeneous nucleation and adsorption: nanoparticles were made as described above. After completion of the reaction, the solution was added to a dispersion of 0.5 g AC in 5 ml water (previously sonicated) and left stirring.

For the one-step synthesis, based on heterogeneous nucleation, the synthesis was scaled-up: 2.0 g of AC was dispersed by sonication in 12 ml water. Then, 0.1315 g silver nitrate was added to form a suspension that was used for the hot injection. The sucrose solution contained 20 g sucrose in 200 ml water for this scaled-up adaptation.

In both cases, vacuum filtration over a Buchner funnel was used to separate the silver coated particles from the reaction solution. The filter paper (Whatman 602 H 1/2) was pre-rinsed with 30 ml demiwater, then the suspension was filtered and the resulting powder was washed three times with approximately 25 ml demiwater. The powder was dried in an oven for 2 hours at 120 °C and afterwards stored in a dark cabinet.

### PVP as stabilizing agent

This experiment is based on the procedure described by Ding et al. [40]. In a typical experiment for a 4 wt% loading, 0.0328 g  $\text{AgNO}_3$  was dissolved in 87.5 ml demiwater in a 3-neck round bottom flask; 0.5 g AC was added to the solution, and the mixture was sonicated for 45 minutes. Next, 17.5 ml of 0.45 M PVP solution was slowly (1 ml per minute) added to the silver solution after the first 10 minutes of sonication. The flask was then connected to a reflux tube and the suspension was heated to 80 °C whilst stirring. Once the dispersion reached the desired temperature, it was kept there for 1 hour while stirring, and then the heating source was removed. The dispersion was left to cool down under stirring. Afterwards, the silver coated particles were separated from the reaction solution using vacuum filtration over a Buchner funnel. The filter paper (Whatman 602 H 1/2) was pre-rinsed with 20 ml demiwater, then the suspension was filtered and the resulting powder was washed three times with approximately 30 ml demiwater. The powder was dried in an oven for approximately 2 hours at 120 °C and afterwards stored in a dark cabinet.

### 3.2.2. Electrodeposition

This synthesis is loosely based on the work by Hong et al. [63]. To prevent a short-circuit by the slurry and enable one-pot synthesis, a dialysis membrane was used. This membrane, a Spectra/Por 7 dialysis membrane with MWCO 50 kD ordered from VWR, was first cut to size for use and placed in demiwater for 30 minutes, to remove the sodium azide it was stored in. After additional rinsing, it was placed in electrolyte solution (0.1 M KOH) for another 30 minutes.

Then, the different electrolytes were prepared for a 4 wt% loading of silver on AC. For the anode side, this involved 5 ml 0.1 M KOH solution with added supporting electrolyte (0.215 g  $\text{KNO}_3$ ). For the cathode side, the electrolyte was made by adding 0.398 g  $\text{AgNO}_3$  to 30 ml 0.5 M  $\text{KNO}_3$  solution (supporting electrolyte). Subsequently, 6.0 g of activated carbon powder was added and the total was sonicated for 30 minutes.

Next, the set-up was built as shown in Figure 3.1. Above a small beaker, the dialysis membrane was hung on a support. Inside, a Pt wire (0.3 mm diameter, 99.9% pure on metals basis, from Alfa Aesar) was connected to the potentiostat as anode. Around the membrane, a coil of Ti mesh (type 10Ti12-125FA, from DexMet) was connected to the potentiostat as cathode. The dialysis tubing was filled to an appropriate level with the anode electrolyte, the beaker was filled to an appropriate level with the cathode electrolyte (not all electrolyte was used). The cathode electrolyte was stirred during the rest of the experiment.

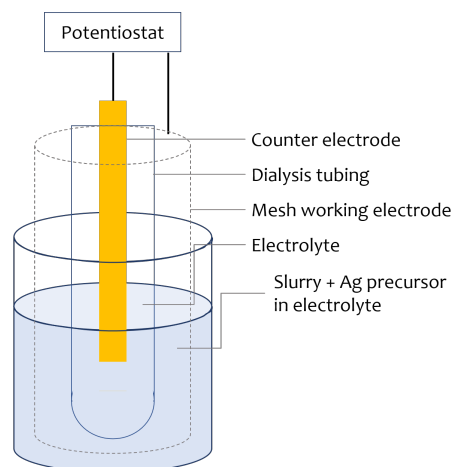


Figure 3.1: Schematic overview of set-up for electrodeposition experiments.

With the potentiostat (Autolab), several CV measurements were taken for later comparison. Then, the potentiostat was set to -5.2 V for 4.5 hours. Afterwards, the cathode electrolyte was vacuum filtered

over a Buchner funnel to separate the activated carbon powder from the reaction solution. The filter paper (Whatman 602 H 1/2) was pre-rinsed with 25 ml demiwater, then the suspension was filtered and the resulting powder was washed three times with approximately 25 ml demiwater. The sample was then dried in the oven for 2 hours.

### 3.2.3. Impregnation

This synthesis is based on the work by Keijzer et al. [64]. In a general procedure for an 8 wt% loading, the synthesis was executed over two different days (consecutive days when possible). On the first day, the silver precursor solution was added to the carbon powder and dried in a vacuum dessiccator. The second day, the powder was reduced under  $H_2$  in an oven.

Four times 1.00 g of activated carbon powder was weighted and brought into four separate vials. An  $AgNO_3$  solution was made by adding 0.5476 g  $AgNO_3$  to 3.0 ml demiwater. Per sample, first 1.8 ml of demiwater and then 770  $\mu$ l of the silver solution was added dropwise. Attention was given to add the liquids dropwise and uniformly, to prevent crusting. Then, the sample was stirred with a glass capillary to assure uniform distribution of the silver precursor. Next, the samples were sonicated for 30 minutes and then placed in a vacuum dessiccator packed in aluminum foil (dark).

For the reduction, the samples were loaded in four ceramic containers (see Figure 3.2 for an example) in such a way that the powder level stayed within the height level of the container. The containers were placed behind each other in the tube oven and the gas flow was turned on (500 ml/min, 15%  $H_2$ , 85%  $N_2$ ). Then the oven was set to 250 °C, with a heating ramp of 3 °C per minute. Once the set temperature was reached, the samples were kept at 250 °C for 2 hours. Then, the oven was shut down and the samples were left to cool down. The  $H_2$  flow was set to 0, while the  $N_2$  flow was kept unchanged.



Figure 3.2: Picture of ceramic sample container used in the tube oven.

## 3.3. Catalytic testing

The catalytic tests were executed using a Teflon flow cell. The cell was assembled using the following layers: Teflon end, carbon paper as current collector, 3 mm plexiglass compartment (see Figure 3.3), Nafion 117 membrane (cation-exchange), Sefar mesh support, 3 mm plexiglass compartment,  $TiO_2$  substrate with  $Ru_2O$ ,  $Ir_2O$  coating as anodic electrode, and the other Teflon end. Silicone gaskets were used to seal all layers together. The cell has an active electrode area of 4  $cm^2$ . The cell was assembled manually with bolts, tightened 2x 1/4 rotation after hand-tightness.

The cathodic reservoir contained a slurry, prepared with 15 wt% activated carbon powder and 85 wt% electrolyte (0.5 M  $KHCO_3$ ). Some activated carbon was coated with silver, in this case the bare carbon weight was considered for making the suspension, to assure similar flow properties. In order to have enough volume for the experiment, the minimum bare carbon weight necessary per sample was around 5 grams. The anodic reservoir contained 0.5 M  $KHCO_3$  as electrolyte. The tubing used has a diameter of around 1/8th inch (3 mm, small variations within sections). The cell was connected to the potentiostat (IviumStat, maximum operation 10V, from Ivium) by electric wires. Two  $Ag/AgCl$  reference electrodes were used to measure the potentials of the individual compartments, as seen in Figure 3.4b. To enable measuring such additional potentials, a peripheral differential amplifier (PDA) box was used (Ivium, maximum 5 V).

During operation, both fluids were pumped at 40 rpm (approximately 10 ml/min in this set-up) with a peristaltic pump (Masterflex L/S, from Cole-Palmer). The complete set-up, as depicted in Figure 3.4a, consisted of two reservoirs with tubing via a pump from the reservoirs to the flow cell and back. The cathodic reservoir was stirred with a magnetic stirrer, to prevent sedimentation of the slurry. The cathodic side of the set-up, including the reservoir, was made gastight and included a connection to a  $CO_2$  cylinder (flow rate  $CO_2$  was set to 50 ml/min) and a gas-outflow to a gas chromatograph (GC, Compact GC 4.0, from Global Analyser Solutions) and a manual flow meter.

In a general experiment, 4 cycles of CV scans from 0 V to -3 V (WE vs CE potentials) were taken

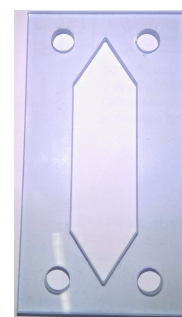


Figure 3.3: Picture of a compartment used in the flow cell.

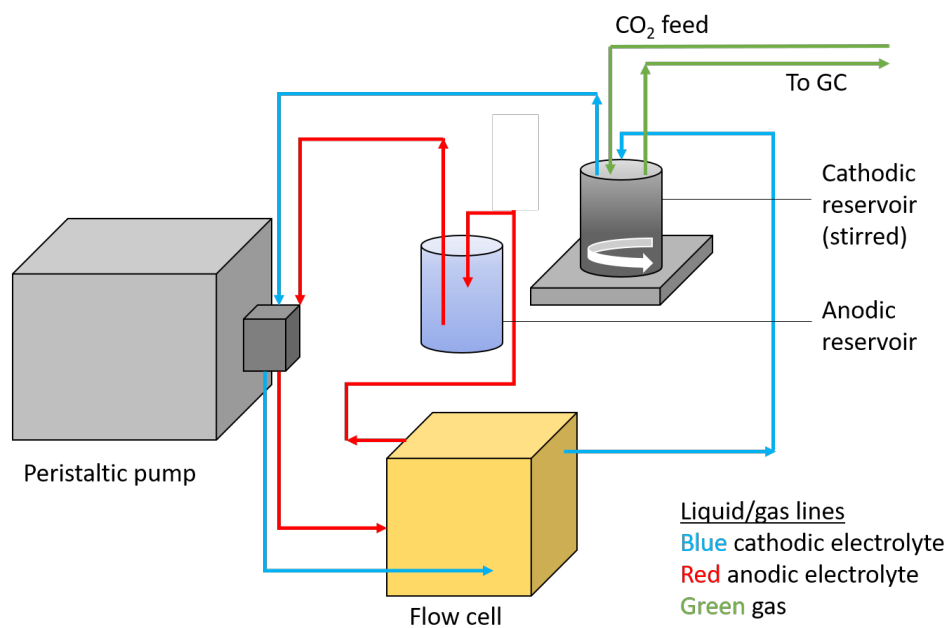
at a scan rate of 100 mV/s before and after the experiment. The catalysis experiment was executed in galvanostatic mode, thus at constant current. After 6 minutes, the first of three GC injections was taken, the others were queued immediately after finishing the previous (one measurement takes approximately 2.5 minutes). In between different current settings, the potentiostat was turned off and then manually set to the next current.

## **3.4. Analysis methods**

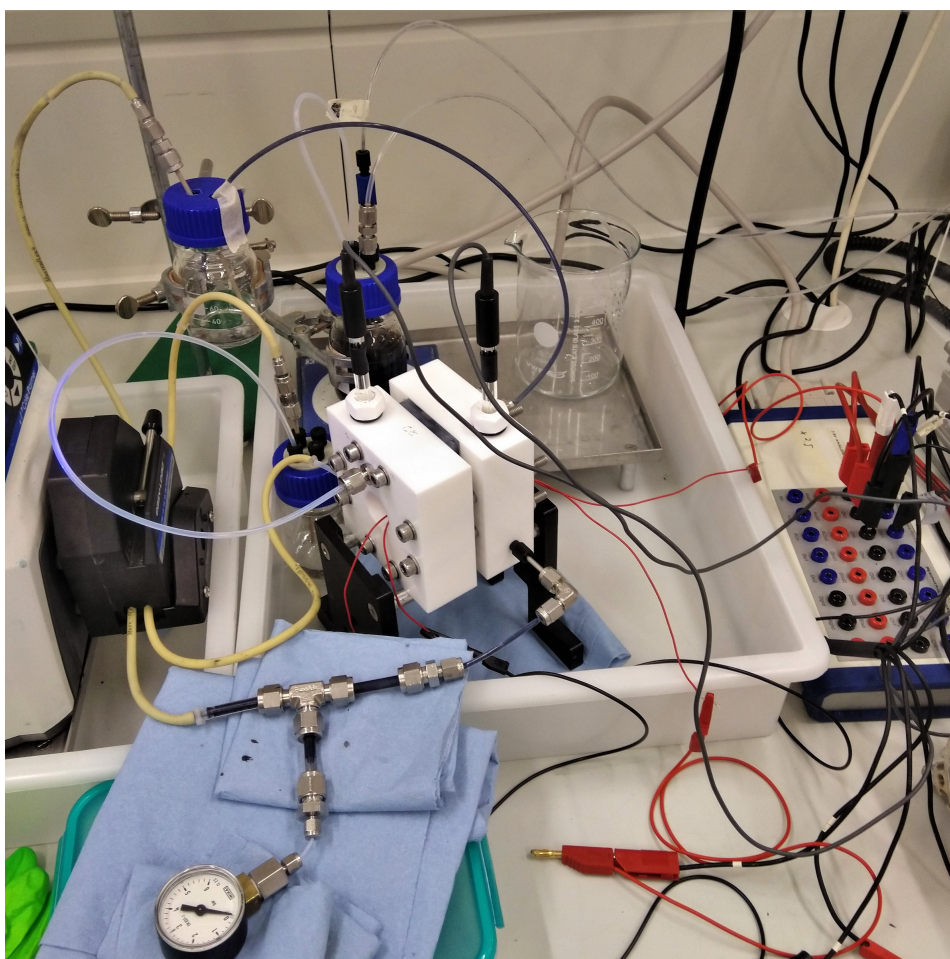
### **3.4.1. ICP-OES preparation**

To determine the silver content on the carbon powders, ICP-OES was used. The measurement of samples was executed by an external technician (instrument: PerkinElmer Optima 5300 with sapphire injector). However, the samples had to be delivered in a specific format, which will be described here. In ICP-OES, it is not possible to measure solids and the best results are obtained when measuring concentration of ions. Thus, the silver nanoparticles had to be destroyed off the carbon particles for this measurement.

In a typical preparation, 60 mg of powder was dispersed in 4.6 ml demiwater and 2.4 ml HNO<sub>3</sub> solution (65-70 %, see section 3.1 for chemicals used). The samples were shaken a few times and left to stand in this acidic solution for a minimum of two hours. Then, they were filtered through filter paper (Whatman 602 H 1/2) and washed with 8 ml of demiwater, making 15 ml of solution. This final solution was handed in for analysis.



(a) Schematic visualization of flow cell set-up consisting of two reservoirs, a pump and a flow cell. The cathodic side was made gastight and the reservoir was equipped with a CO<sub>2</sub> inlet and an outlet to a GC.



(b) Photo of the set-up used, with the flow cell, pump, tubing, reservoirs and connections. This photo was taken during clean-up procedure, hence the cathodic reservoir with the slurry is not connected.

Figure 3.4: Visuals of the set-up used in catalysis experiments.



# 4

## Results and Discussion

Silver nanoparticles on the activated carbon support were synthesized using five different methods: impregnation, electrodeposition, AC only, PVP and sucrose. In Section 4.1, the results of these syntheses are described by the deposition efficiency, particle size, stability and practical arguments, showing that impregnation and electrodeposition are the most suitable for this application.

These two samples and a blank (no silver) were prepared into a slurry and then tested for catalytic activity in a flow cell. In Section 4.2 it is discussed that these experiments required a very high cell potential and showed unexpected trends for CO flow related to current density, bringing to question how the CO is formed, since CO<sub>2</sub> reduction seems unlikely based on the data.

### 4.1. Synthesis of silver nanoparticles

The synthesis methods were selected for their assumed ability to deposit silver nanoparticles of sizes 5-20 nm in an efficient manner on AC (refer to Section 2.3 for more information about the different methods). The results for both the 1-step and the 2-step sucrose method are shown combined to keep the overview more simple, as these results were fairly similar. Besides the results shared in this section, the oxidation state of the silver nanoparticles was also measured using XPS and can be found in Appendix A.

Figure 4.1 shows TEM images of samples produced with different synthesis methods. The methods, from a to e, are: impregnation, electrodeposition, AC only, PVP and sucrose. In Figure 4.1a, c-e the scalebar is 200 nm, in b the scalebar is 100 nm. All images show mainly near-spherical particles, although large blocks are visible as well in c and d.

The impregnation sample shows a higher density of particles than all the other samples. It was synthesized at 8 wt% silver and the other samples at 4 wt%, but the content difference appears to be more than twice, which suggests a higher deposition efficiency. The impregnation sample has particles through the entire depicted carbon substrate, whereas for the other samples the particles are mostly visible around the thinner carbon regions.

The sample produced with only AC has a few small particles visible and large black blocks. The blocks are most likely bulk silver, because of the well-defined borders, but could potentially also be thicker carbon. Since there was no strong reductant present in this synthesis, larger particles are more sensible: nucleation is slow due to the lack of reductants, and all silver that gets reduced most likely sticks together due to the absence of any stabilizers. The other three samples, produced by electrodeposition, PVP or sucrose, all have a clear presence of nanoparticles, but in lower quantities.

What should be noted about TEM images is that only few individual carbon particles are studied. The detail of the gathered information is high, but the sampled amount is very low and thus might not necessarily represent the total sample. Therefore TEM images are only used to study particle size distribution in this thesis (see Subsection 4.1.1) and a more quantitative method (ICP-OES) is used to accurately determine the silver content (see Subsection 4.1.1 and 4.1.3). The analysis of these methods combined to determine which synthesis method is most suitable can be found in Subsection 4.1.4.

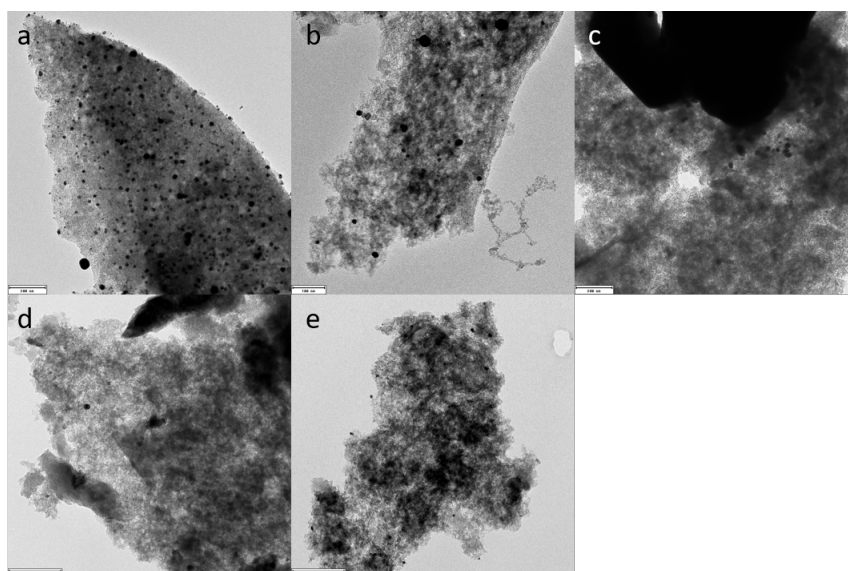


Figure 4.1: TEM images of silver nanoparticles (black) on an AC support (gray), produced by different synthesis methods. Synthesis methods: a) Impregnation, b) Electrodeposition, c) AC only, d) PVP, e) Sucrose. The scale-bar is 200 nm, except for image b (100 nm).

#### 4.1.1. Silver content

An important measure in determining the success of the synthesis method is the yield of silver on the carbon particles. Therefore, the silver content was measured using ICP-OES, as explained in Chapter 3. Figure 4.2 shows the silver content of samples produced by different methods and the efficiency of the deposition, calculated as the percentage of silver deposited from the total amount of silver available during the synthesis.

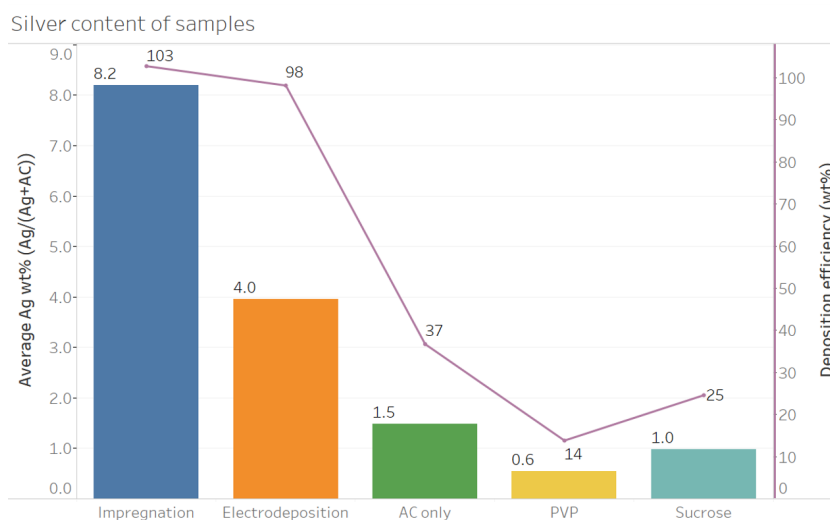


Figure 4.2: Silver content on carbon samples. Each color represents a different synthesis method. The bars show the average silver content of the samples, expressed as the mass of silver per mass of silver and carbon combined. The purple line shows the efficiency of the deposition, calculated as the percentage of silver deposited from the total amount of silver available. Both impregnation and electrodeposition lead to samples that have almost all available silver present within the sample. Samples produced with PVP, sucrose or without reductant have a lower deposition efficiency.

These deposition results immediately visualize inherent differences between different synthesis methods. Interestingly, the samples produced with an agent present (PVP, sucrose) have an even lower silver content than the sample without an added reductant or stabilizer (AC only). The silver yield of the AC only sample is limited to 36%, likely because the carbon powder by itself is not a great re-

ductant. Nevertheless, it is also the only reductant present in that sample, thus silver is mostly reacting at the carbon surface. With the lack of stabilizers, the carbon surface is also the only heterogeneous nucleation site available, thus there are two reasons that make it more likely that the particle stays on the surface instead of being loose in solution.

The PVP and sucrose methods have a lower deposition efficiency. The presence of stabilizers in solution and supported reduction reduces the driving force for particles to deposit on the carbon surface. This might explain why the main part of the silver did not end up on the particle.

Electrodeposition does a better job of putting the silver on the particle, with an efficiency at nearly 100%. This can be explained with the fact that the method puts a potential on the particles, which acts as a driving force for the silver to react at the particles' site.

The highest silver content is found with impregnation, giving an average efficiency of over 100% for an 8 wt% loading. A percentage of over 100% seems impossible, but this is most likely explainable with local differences in the sample. Since only a small sample of the powder is used for the silver content determination, it is possible that the sample is not perfect representation of the total sample. Taking multiple samples could give a more accurate determination of the silver content. Nevertheless, the high silver content is related to the synthesis method. In this method, solvent volumes are kept to a minimum and they are evaporated before the formation of the nanoparticles. Because the nanoparticle synthesis takes place with a dry powder, no washing steps are needed. Thus there are two reasons that explain the high efficiency of this method: no silver is lost with the solvent and no silver is lost with washing.

#### 4.1.2. Particle size distribution

Another aspect to determine the quality of the synthesis methods, is the size of the produced particles. As explained in Section 2.3, the ideal particle size is 5 nm, but the range 5-20 nm will produce particles that are catalytically highly active. To determine the particle size of the synthesized silver particles, TEM photos were taken and particles were measured by hand using ImageJ.

Figure 4.3 shows the average particle size (bars) with standard deviation (represented as error bars) for the same synthesis methods as in the above section (the particle size distributions, including the count per sample, are included in Appendix A). Here it is visible that both impregnation and electrodeposition result in similar particle size distributions. To produce smaller particles, the sucrose method is more suitable. Both the PVP synthesis and the synthesis without reductant lead to larger particles, although even those are still close to the desired range.

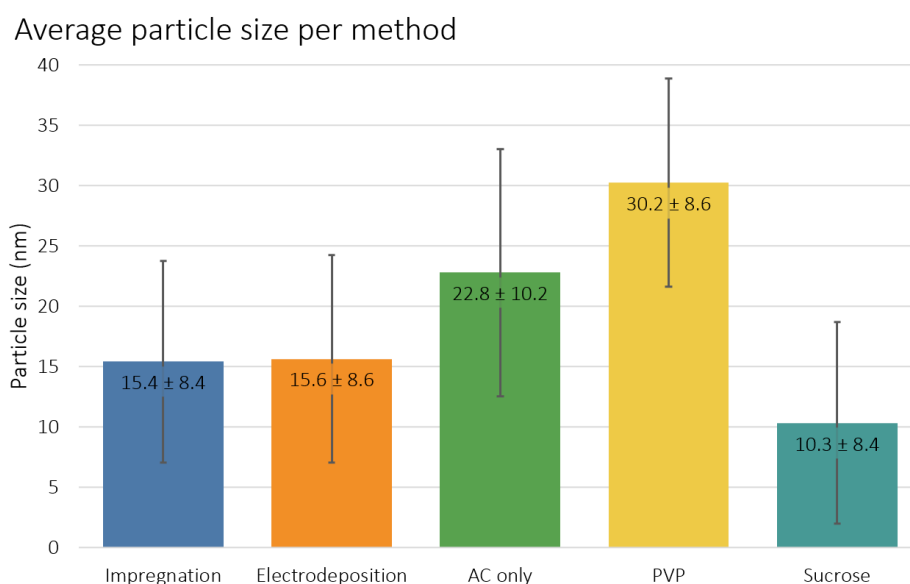


Figure 4.3: Average particle size with standard deviation per synthesis method. The smallest particles (10 nm) are produced with sucrose as reductant. Both impregnation and electrodeposition lead to slightly larger particles of 15 nm. With PVP as reductant, the particles are the largest (30 nm). All samples have a similar standard deviation.

The accuracy of these particle size measurements is debatable. Since they are measured by hand, small inaccuracies are made and this causes the deviations to be larger. Additionally, very small particles (<3 nm) are hard to observe on the carbon support background and thus not present in the measurements, very large particles, >100 nm, are generally also excluded, since it could be that the observed spots are not silver particles. The TEM only gives a visual image of electron resistance and large black spots can also be a dense portion of carbon. Because of these discrepancies the particle sizes measured are naturally more close together, and thus the results are not a perfect description of the samples.

#### 4.1.3. Stability of produced catalysts

To find out how durable the produced catalysts are, their silver content was also measured after the catalysis experiments (the results of the catalysis experiments follow later, in Section 3.2). For these experiments, both the impregnation and the electrodeposition samples were used, as well as a blank sample without any silver. For proper comparison, it should be noted that the electrodeposition sample was used twice and was diluted 1 to 1 with bare carbon powder in one for these experiments, thus a 2 wt% loading is expected. In Figure 4.4 can be seen that the majority of silver is still present on the powder for both the electrodeposition and the impregnation sample. For the electrodeposition sample, 102% residual silver was measured. There are two possible explanations for this. Firstly, as mentioned before, only a small powder sample is taken for the ICP-OES measurement and silver distribution on the powder is not necessarily even. Additionally, the dilution of the sample for use in the catalysis experiment was not measured accurately, and thus the 1 to 1 ratio is an estimation and the real dilution can be slightly different.

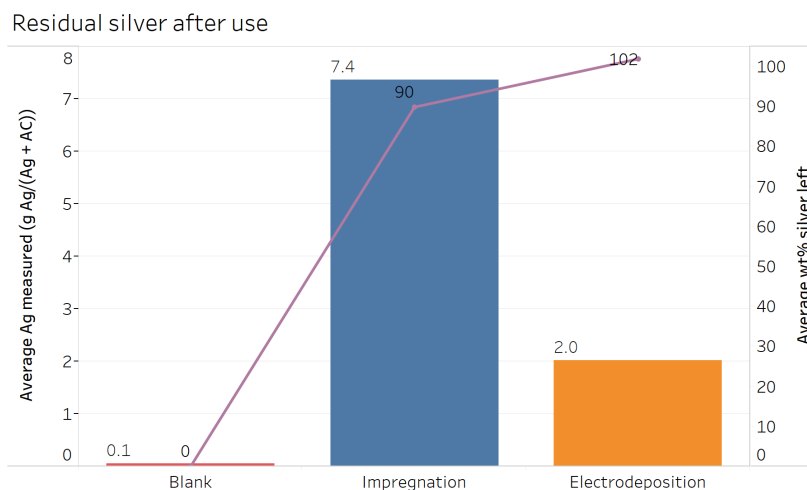


Figure 4.4: Residual silver on samples after use in a flow cell. The height of the bars shows the silver amount measured in the solid phase, expressed as silver mass per mass of silver and activated carbon. The line refers to the residual silver as well, but now expressed as a percentage of silver present after synthesis.

In the impregnation case, there is a loss of 10% of silver after use in only one experiment. Looking ahead to future applications with much longer running times, this could be a potential problem. One explanation for this difference could lie in the fact that the impregnation sample has not undergone any washing/filtration in synthesis and thus maybe any loose silver is washed away during the experiments. Alternatively, there could be a difference between on what sort of sites the silver is deposited, such as on the outer particle versus in the pores and as a result, more silver can be lost or kept. Thirdly, some silver is deposited as  $\text{Ag}_2\text{O}$  (see Appendix A), which is firstly reduced to  $\text{Ag}^0$  upon use as cathode. This change in composition results in size change of the particle and can also be a cause of silver loss. For a more accurate determination of the deposition stability, more detailed tests need to be done, for example one that measures the losses at different running times.

Interestingly, the presence of silver was also measured on the blank sample, although it was a very small amount (0.1 g Ag / g (Ag + AC)). This shows that some contamination is taking place, most likely due to sample being left behind in the flow cell after use.

#### 4.1.4. Discussion on preferred synthesis method

Combining the deposition amount and efficiency, particle size and deposition stability, impregnation is the most suitable method, although electrodeposition is also promising. Both electrodeposition and impregnation show approximately 100% of silver deposited, and more than 90% remaining after use in the flow cell. Both also have a similar particle size distribution that matches well with the desired size. For electrodeposition, no 8 wt% samples were made, thus it would be inaccurate to rule it out based on the absolute higher loading of impregnation. The syntheses with AC only, PVP and sucrose disappointed in the amount of silver deposited on the particle and have little to no benefits to compensate for this.

Nevertheless, other, more practical arguments should also be considered; for example, how facile the synthesis is executed, how high the yield is, if there are still options for modification of the size and shape of the nanoparticle and to what extent the method is scaleable. Impregnation synthesis is executed over two consecutive days and that is surely a disadvantage. It also requires the use of a more complex piece of equipment, a tube oven under  $N_2$  and  $H_2$  atmosphere, which is not present in the group for use, making it less practical for more intensive use. Electrodeposition on the other hand is easily executed in a fume hood within one day, although building the set-up requires a much higher level of precision and attention. For example, in an earlier electrodeposition experiment, an electrode burned a hole in the membrane, ruining the experiment, but due to the opaque, black solution, this was only discovered upon disassembly.

In terms of versatility of the syntheses, the impregnation synthesis can be adapted to melt impregnation for an even higher silver loading, although one might wonder if such a high silver loading is necessary in this set-up. It is difficult to compare the silver loading on a carbon substrate versus a regular flat electrode and thus to determine how much silver is necessary to assure it is not the limiting factor for  $CO_2$  reduction. Alternatively, small modifications to the electrodeposition synthesis enable changing the shape of the nanoparticles, for example to produce higher surface area dendrites, instead of spheres.

Impregnation provides a yield of 4 grams of powder, electrodeposition results in 5 g of powder, but both of these are not enough to make a suitable slurry volume for experiments in the flow cell. To scale up the impregnation procedure for a satisfactory yield at the laboratory scale, a larger tube is required that can hold more powder and thus more boats (preferably 8 or more). This is not possible in the current set-up, but is feasible in case a different tube oven is built. For electrodeposition, scaling can be realized in a more simple manner by using a larger beaker, mesh and dialysis tube. However, in a larger solution the reaction kinetics might differ and could potentially lead to inferior results.

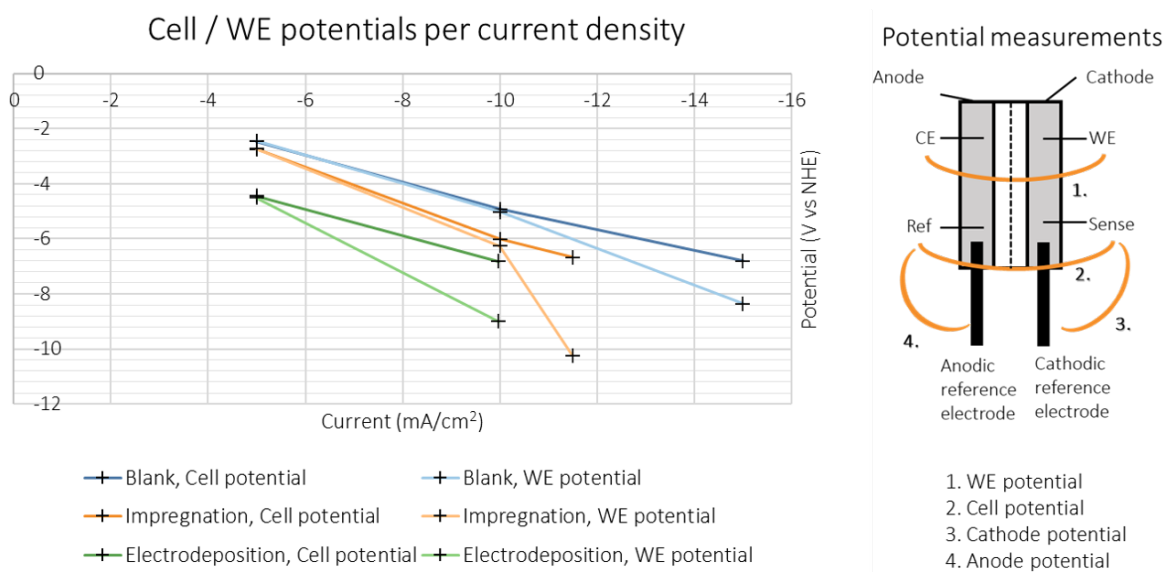
## 4.2. Catalysis experiments

Using the samples with a silver catalyst in a flow cell, the aim was to produce CO by reduction of CO<sub>2</sub>. In this experiment, three slurries were studied: one based on the impregnation sample, one based on the electrodeposition sample and a blank with bare AC, thus without silver present. All measurements were executed in order of increasing absolute current density.

### 4.2.1. Flow cell electrochemistry

To achieve the desired currents during the catalysis experiments, high potentials were required, as seen in Figure 4.5a. This figure is derived by averaging the measured current and potential after 100 seconds from the time dependent data measured in the experiment. The experiments were set at constant current, starting at -5 mA/cm<sup>2</sup> to -10 mA/cm<sup>2</sup> and -15 mA/cm<sup>2</sup>. However, since the working electrode potential reached the potentiostat's maximum controllable potential (-10 V) during some measurements, the potentiostat was not always able to reach the expected currents. Therefore there is a data point for -11 mA/cm<sup>2</sup> in the blank experiment instead of -15 mA/cm<sup>2</sup>, for the same reason, -15 mA/cm<sup>2</sup> was not even measured anymore for the electrodeposition experiment.

Particularly at higher currents, the potential measured seems excessive for the reactions desired. The measured cell potentials (measured over the sense and ref, as seen in Figure 4.5b) range from -3 V at -5 mA/cm<sup>2</sup> to -7 V at -15 mA/cm<sup>2</sup>, and the potential over the working electrode (measured over the WE and CE, as seen in Figure 4.5b) even reaches up to -10 V (maximum of potentiostat) at higher currents. From this point onwards, the potentiostat cannot control the current well and thus data is unreliable at best, most likely explaining the deviations between the WE potential and cell potential observed at the higher current measurements.



(a) Average potential after 100 s over WE/CE and SENSE/REF (=cell potential) plotted against the average current density during catalysis experiments. The darker colors show the cell potential and the lighter colors show the WE potential. The measured WE potential is equal or higher than the cell potential, both potentials are increasing with current. Color represents the sample used in the experiment.

(b) Schematic overview of electrode connections for the measured potentials.

Figure 4.5: Potentials measured during catalysis experiments. In a, the average measured potential after 100 s is plotted against the current density. In b, the different potentials measured are schematically visualized for clarity.

High potentials are the result of high resistance within the system, which prevents the electrons from reacting as expected. In this slurry flow cell, high electron transfer resistance between the electrode and the slurry could well be the cause of this, as they are the main 'new' addition. At this point, however, it is yet unclear where the source of this high resistance lies.

Further research into the source of the resistance shows that the problems are mostly occurring on the anodic side of the cell. The anode and cathode potentials, measured separately against a reference electrode during the same experiments, are shown in Figure 4.6. The anodic potentials are positive and thus plotted > 0 V vs NHE, the cathodic potentials are negative and plotted < 0 V vs NHE. This plot

shows the cause of the increasing cell potentials to be on the anode side of the cell, not the cathode. This is rather unexpected, as the anode side is employed with a  $\text{Ru}_2\text{O} / \text{Ir}_2\text{O}$  catalyst that is known to effectively catalyze the OER (occurring at 1.23 V vs NHE) at low overpotentials [65]. In contrast, the cathode potential needs barely -1 V at  $-15 \text{ mA/cm}^2$  to promote the  $\text{CO}_2\text{RR}$  (occurring at  $-0.1 \text{ V}$  vs NHE).

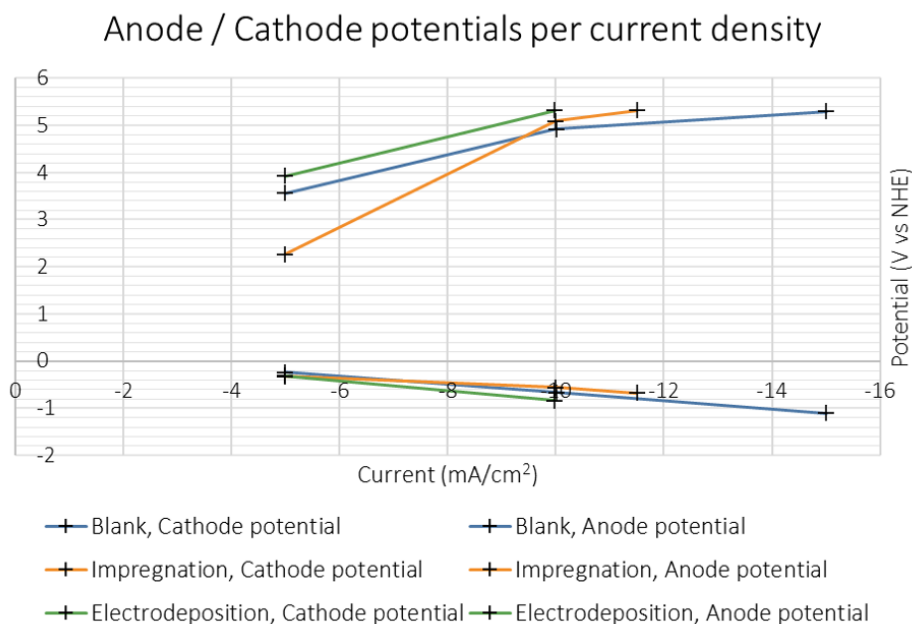
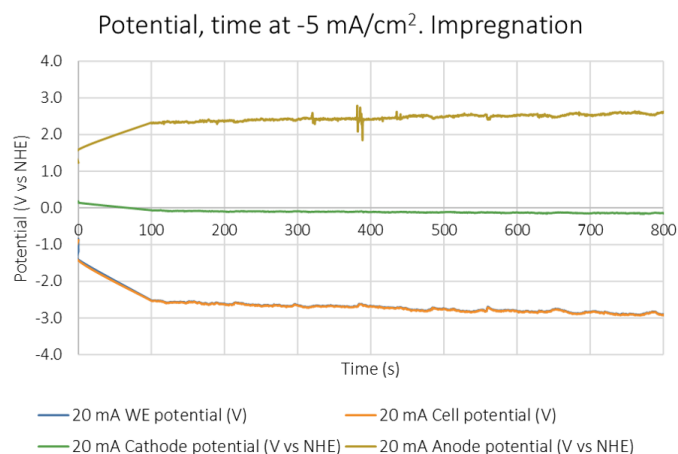


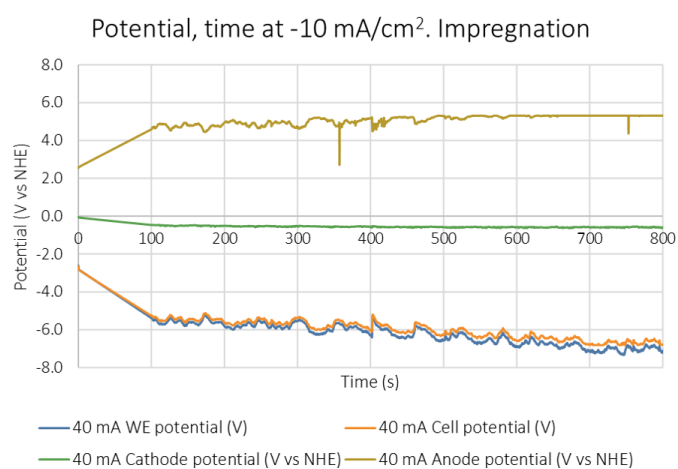
Figure 4.6: Measured anode and cathode potentials during catalysis experiments. Anodic potentials (positive) increase more than two-fold within the measured current range to 5V versus NHE. Cathodic potentials (negative) barely increase with increasing current density. Color represents experiment.

For a closer look at what is happening on the anode, potential over time diagrams are included in Figure 4.7 for the impregnation experiment. The graphs for the other two experiments are included in Appendix B. These potential over time graphs show more clearly what happens at the different locations in the cell. Firstly, the WE potential and cell potential are equal at  $-5 \text{ mA/cm}^2$ , have a slight deviation at  $-10 \text{ mA/cm}^2$  and then have a 3 V difference at  $-11 \text{ mA/cm}^2$ . In Figure 4.7a and 4.7b, all four measurements show some degree of noise, as expected in a real measurement. However in Figure 4.7c, there is no more noise visible in the measurements for both the anode and the WE potential. The apparent limit of 5 V for the anodic potential is most likely explained by the limit of the PDA box used, which is also 5 V. Nevertheless, this limit should not have impacted the rest of the experiment, since this information is only noted as data, not instrument control.

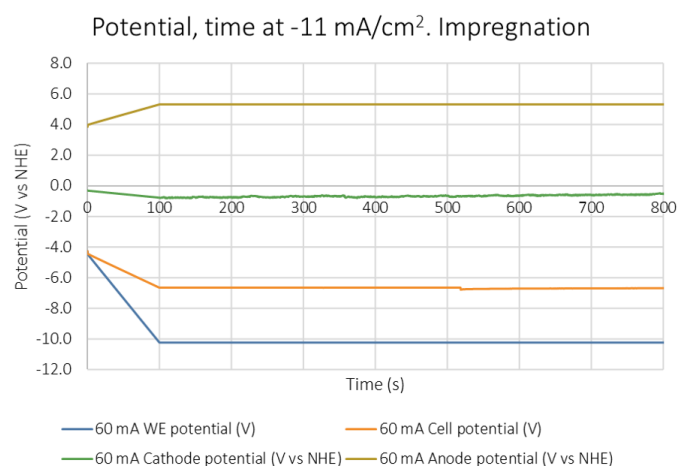
An additional observation can be made from these graphs; namely that the measured cell potential is not exactly the difference between the cathode and anode potential. This is explained because two separate reference electrodes are used. Both of these are used separately to measure the potentials in the individual compartments, but the combination of these does not take into account a piece of the electrolyte and the membrane. Therefore, the measured cell potential is higher than the sum of the individual pieces.



(a) Potential over time measurements during catalysis experiment at  $-5 \text{ mA/cm}^2$ . The different potentials measured are: WE potential (blue,  $-2.7 \text{ V}$ ), cell potential (orange,  $-2.7 \text{ V}$ ), cathode potential (green,  $-0.1 \text{ V}$ ) and the anode potential (olive,  $2.5 \text{ V}$ ).



(b) Potential over time measurements during catalysis experiment at  $-10 \text{ mA/cm}^2$ . The different potentials and their average value measured after 100 seconds are: WE potential (blue,  $-6.3 \text{ V}$ ), cell potential (orange,  $-6.0 \text{ V}$ ), cathode potential (green,  $-0.6 \text{ V}$ ) and the anode potential (olive,  $5.1 \text{ V}$ ).



(c) Potential over time measurements during catalysis experiment at  $-11 \text{ mA/cm}^2$ . The different potentials measured are: WE potential (blue,  $-10.2 \text{ V}$ ), cell potential (orange,  $-6.7 \text{ V}$ ), cathode potential (green,  $-0.7 \text{ V}$ ) and the anode potential (olive,  $5.3 \text{ V}$ ).

Figure 4.7: WE, cell, cathode, anode potential over time measurements from catalysis experiment with impregnation sample at different current densities.

Looking at the cause of the high anodic potentials, there are a few sources of resistance possible. Because this is a flow cell, bulk mass transfer for water is unlikely to be a problem, as the electrolyte is constantly flowed by the electrode. Electron transfer at the electrode surface and chemical reaction are not expected to be the source of the problem either, since the electrode used is a common catalyst for OER under mildly basic conditions. Nevertheless, it might be worth verifying its quality as this would well explain the observed problems. Ionic resistance of the electrolyte was not measured separately and can also play a role resistances, although an 0.5 M solution of  $\text{KHCO}_3$  is a commonly used electrolyte, thus severe problems from its ionic resistance are unexpected. Another source of resistance can be absorption and desorption of gases, in this case the desorption of oxygen gas. Gases can be a source of resistance in two different ways: gas molecules can occupy electrode sites and thus block the reaction, or gas bubbles can block the ion transport from and to the electrode thus increase electrolyte resistance, the latter of which is a commonly observed problem [66]. Looking at cell performance of time might help to identify which of these aforementioned possible explanations are the cause of the problem.

Before and after the catalysis experiments, cyclic voltammetry (CV) scans were taken to investigate cell degradation over time. In CV, the potential over the WE is varied while the current (and cell potentials) are measured. Figure 4.8 shows a combination of the CV scans of the three different experiments before (blue) and after (orange) the catalysis measurements, in order of execution (a to b to c). For all three experiments, a minimum two-fold decrease in current is observed between the measurements before and after the experiment. Before the catalysis experiments, a clear reaction current is observed after 1.2 V vs NHE, whereas after the catalysis experiments, this reaction current has decreased, indicating that the anode was at least partially disabled irreversibly during the experiment.

Still, two potential causes can be named to explain the observations: oxygen bubbles blocking access of the electrode or catalyst degradation. The latter of which would be observed as degradation over experiments as well. This would mean that the current observed in the 'after' measurement of the impregnation experiment, is similar to the current observed in the 'before' measurement of the blank experiment, and equally so for the measurements after the blank sample and before the electrodeposition sample. This is not true for the first combination, however it does fit for the latter. Based on this data, catalyst degradation cannot entirely be excluded, but it seems more likely that oxygen bubbles are the problem than catalyst degradation. Between the experiments, there is one other variable that was not entirely constant, namely the composition of the anolyte. It was not refreshed between the experiments, only refilled when needed. This can also have influenced the results, as the solution is acidified during the reaction.

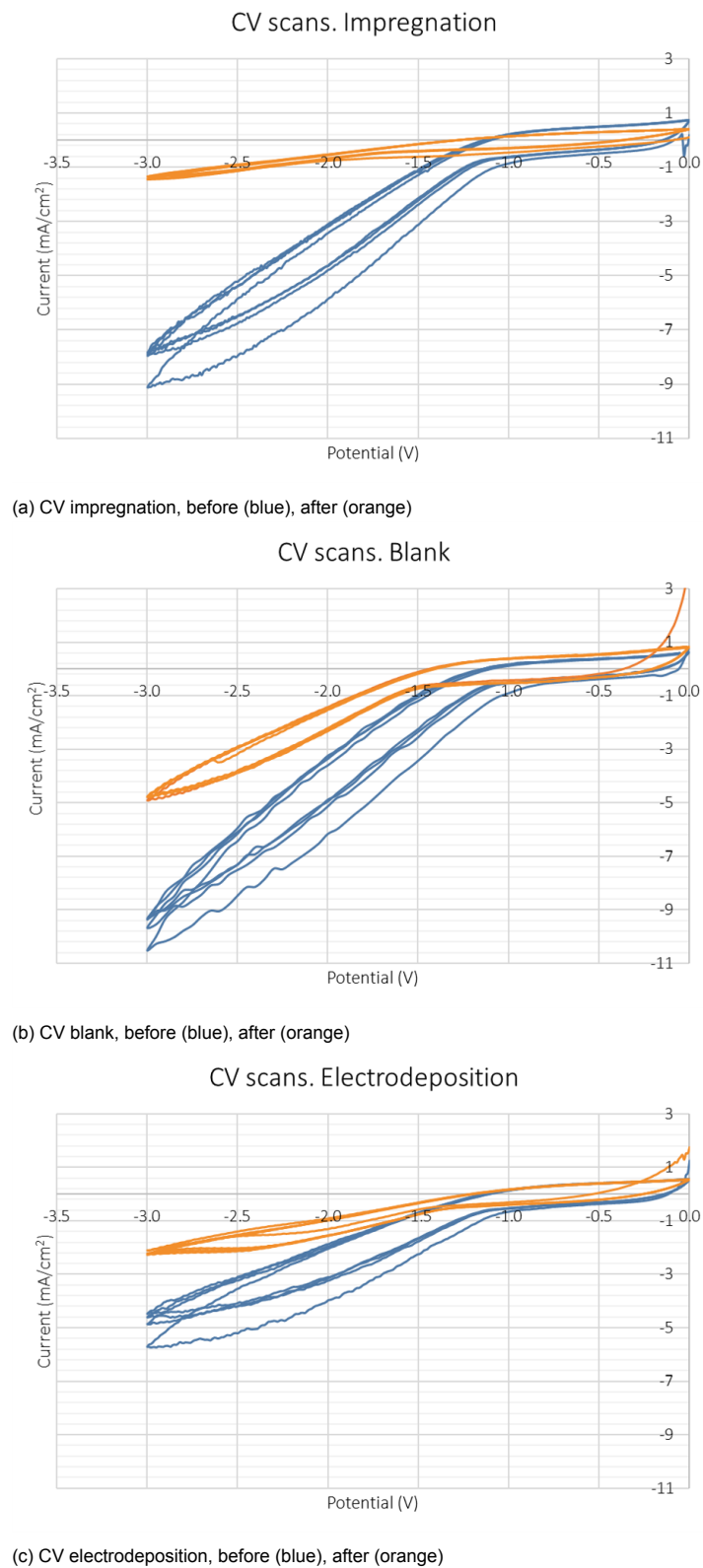


Figure 4.8: CV scans of the three catalysis experiments, executed before (blue) and after (orange) the catalysis measurements. Included in order of execution, a to b to c.

### 4.2.2. Reaction product analysis

To investigate more closely what electrode reactions took place at the cathode, the outgoing gases were measured in a GC. For all samples,  $\text{CO}_2$  was the main component (this data can be found in Appendix B). The presence of  $\text{O}_2$  and  $\text{N}_2$  was measured as well, yet no  $\text{H}_2$  was detected. Per set current, usually three data points for the GC were taken, with the exception of the blank experiment at  $-5 \text{ mA/cm}^2$ , where one less data point was obtained. For all sets, the first GC measurement showed no presence of CO, although the subsequent ones always detected CO. It is reasonable that the gas headspace was not entirely refreshed with the new sample at this time and thus the first measurement of each set was excluded. The other two data points (one for blank at  $-5 \text{ mA/cm}^2$ ) were converted from CO concentration into CO flow, averaged and shown in Figure 4.9, for the blank experiment and the two catalyst experiments.

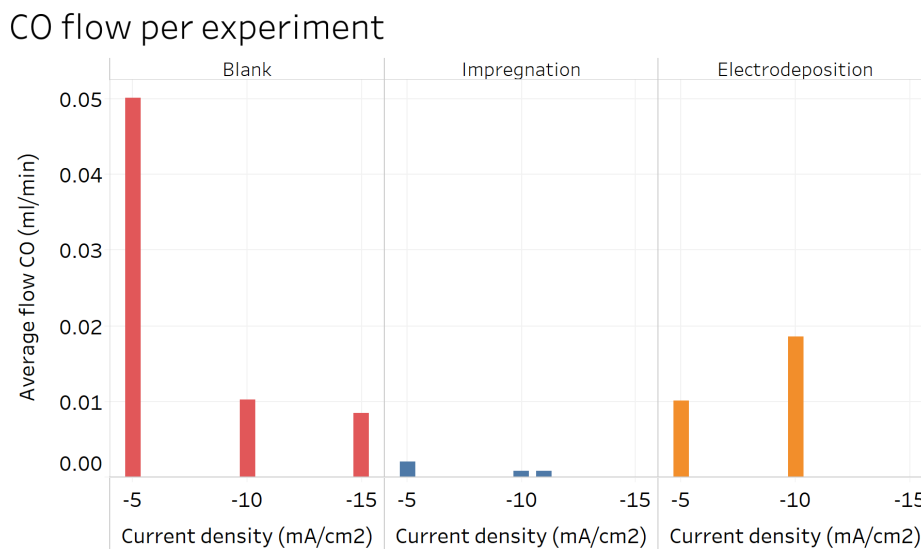


Figure 4.9: CO flow rate at current density, per sample. The experiment with the highest CO production is the blank sample at low current density. The two experiments that follow, have a much lower (-80%) CO production. For the electrodeposition sample, the CO flow rate doubles with double the current density. For the impregnation sample, the CO flow rate is nearly negligible at all current densities.

Presence of CO is measured during the all measurements, which is against expectations. For  $\text{CO}_2$  reduction normally a catalyst is necessary, which was not deemed present during the blank experiment. Also important to note, is that this CO flow is decreasing with current density, whereas normally the production of reduction reactions is increasing with current density (as observed for the electrodeposition sample). Those arguments combined make it very unlikely that this CO is produced by  $\text{CO}_2$  reduction.

Between the slurries coated with silver, the CO flow for the electrodeposition sample is measured to be higher than for the impregnation sample, which is particularly interesting considering that the electrodeposition sample for the catalysis experiment consisted of only for half of its contents out of a coated sample (the other half was bare carbon powder, due to a lack of more coated powder). Also, this sample had been used in a flow cell experiment before. As it seems, the presence of the catalyst is not a determining factor here either.

Additionally,  $\text{H}_2$  is normally also present as a reaction product, as the reaction potentials for the  $\text{CO}_2\text{RR}$  and the HER are very similar. However, in these experiments no presence of  $\text{H}_2$  was measured. This could be due to the low sensitivity of the GC to  $\text{H}_2$ , but previous experiments (not included here), showed presence of  $\text{H}_2$  with only the change of current collector at similar current densities.

Based on the measured CO flows and electrochemistry data, the Faradaic efficiency for  $\text{CO}_2$  reduction to CO is calculated and shown in Figure 4.10. It can be seen that all Faradaic efficiencies are very low, with the exception of one (33% in the single blank measurement at  $-5 \text{ mA/cm}^2$ ). This means that, even if the observed CO is produced from  $\text{CO}_2$ , there are still many electrons unaccounted for, although at this stage it is difficult to say where they went, especially due to the absence of other measured reaction products.

## Faradaic efficiency for CO per experiment

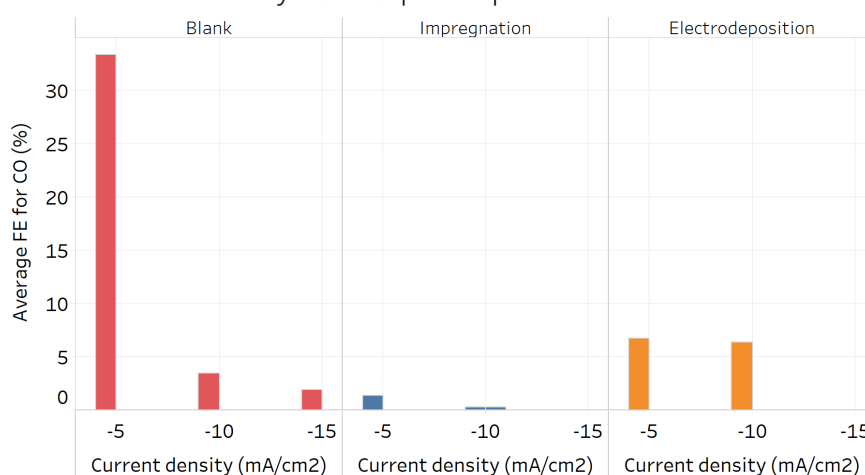


Figure 4.10: Theoretic Faradaic efficiency of CO production at current density, per sample. The highest FE observed is 33% for the blank sample at  $-5 \text{ mA/cm}^2$ . All other FEs are below 10%.

To explain the results as seen, there must be another source of CO, other than  $\text{CO}_2$  reduction. Since the GC measures the composition of the gases on the cathodic side of the flow cell, the anodic problems described in Section 4.2.1 cannot be an explanation. The cathodic side of the cell has multiple carbon sources, both the carbon powder and the carbon paper current collector. It is possible to produce CO from carbon by oxidation, although seemingly unusual at a cathode. Alternatively, there could be CO bound to the carbon particles, that is released during the catalysis experiment. This would also explain the differences between the bare and the coated samples: possibly, the CO in the coated samples has already been released during synthesis.

To verify this second hypothesis, XPS data on the oxidation state of carbon has been obtained and shown in Figure 4.11. This data immediately shows that the above hypothesis, that already present C-O is released, is likely untrue. There is no noticeable difference between the samples that have been prepared and the bare AC. Thus, the source of the CO is yet to be found. More on how this source can be identified and how to work towards proof of  $\text{CO}_2$  reduction will be discussed in Chapter 5.

## Carbon oxidation states distribution

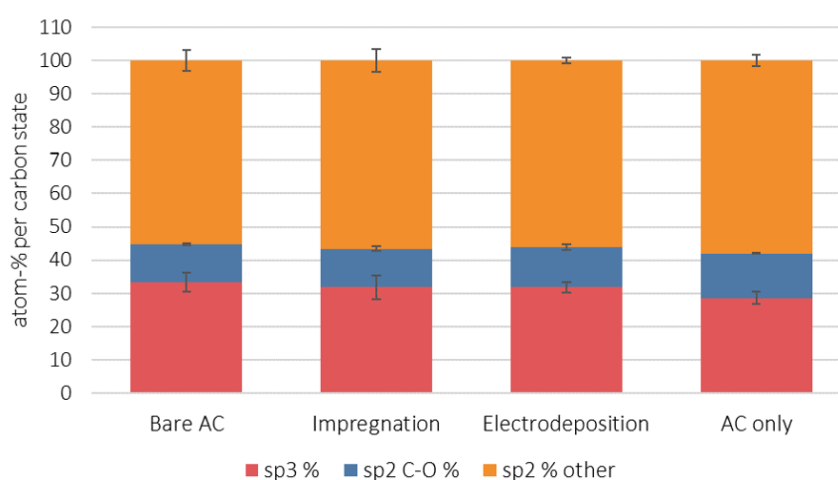


Figure 4.11: Carbon oxidation states in atomic percentages per sample, measured after deposition of silver (except for bare AC, which did not undergo any synthesis). All four samples show a similar distribution between  $\text{sp}^2$  and  $\text{sp}^3$  carbon. Also their amount of carbon bonded to oxygen is similar.

# 5

## Conclusions and Recommendations

### 5.1. Conclusions

The thesis was executed with two goals in mind: synthesis of silver nanoparticles on activated carbon support and testing of their slurries' catalytic activity for CO<sub>2</sub> reduction in a flow cell. A list of main observations and conclusions is found here.

1. Both electrodeposition and impregnation yielded powders with a near-100 wt% deposition efficiency, with silver nanoparticles of 15±8 nm and more than 90 wt% silver remaining after use in a slurry experiment, thus they are suitable deposition methods.
2. During electrolysis experiments, an unusually high potential was needed to reach a reasonably set current. The cause of this lies within the anode side of the cell and is irreversible within an experiment, but disappears in between different experiments, thus is most likely related to oxygen bubbles.
3. In those same experiments, the presence of CO was measured in experiments with silver catalysts but also in the blank experiment. Therefore, it is unlikely that this was produced by CO<sub>2</sub> reduction at this point.

#### 5.1.1. Successful synthesis of nanoparticles

For the nanoparticle synthesis, the aim was to produce silver particles on the activated carbon support between 5-20 nm in size and a high deposition efficiency and stability. Both impregnation and electrodeposition satisfy those requirements and are thus suitable deposition methods for creating silver coated carbon particles to use as slurry electrodes.

#### 5.1.2. Poorly functioning anode

During the catalysis experiments, high potentials were needed to reach reasonable currents. The cause of this was found to lie on the anode side of the cell, and is irreversible within an experiment, yet disappears in between different experiments. This seems most fitting for a problem that is solved upon disassembly of the cell and the most likely cause of the poor cell functioning was therefore identified to be resistance induced by oxygen bubbles.

#### 5.1.3. Questionable CO<sub>2</sub> reduction

The original aim of the catalysis experiments was to study differences in catalytic properties between the produced catalysts. The obtained results do not prove that any CO<sub>2</sub> reduction has taken place and thus any analysis of catalytic properties between the samples is not useful.

Nevertheless, the results show an interesting relation between CO production and the current density, that cannot be explained entirely to this point. One hypothesis was that the measured CO was already present at the carbon particle's surface and released during the experiments, but this was already proven not to be true. Alternatively, oxidation of carbon can also produce CO, although more research needs to be done to find out how and why that is happening and what to do about it.

## 5.2. Recommendations

### 5.2.1. Nanoparticle deposition in final application

For this project, the efficiency of the method was more important than actual amount of deposited silver. At a later stage, it can be worth experimenting with the silver loading, to assure that the silver amount is not the limiting factor for the reaction.

Additional factors affecting future use of the synthesis methods are the yield and versatility of the method. Particularly the scalability of that yield is important for future applications, which was not studied in detail, but only shortly discussed in earlier chapters. Since it is the eventual goal to use slurry electrodes for larger scale operation, it is important that the synthesis method allows for scaling up. In the short term, scaling electrodeposition would mean scaling the beaker and electrodes. It appears easily scalable for a small range of sizes and manual operation, yet more complex for industrial application, although using a fluidized bed reactor would possibly create options. Impregnation on the other hand seems a more sensible choice for industrial applications, and is commonly referred to as a method used at industrial scale. For the short term however, scaling this method would involve building a new tube oven, which is rather a lot of work for laboratory application.

In terms of versatility, electrodeposition is known to be used for synthesis of dendrite particles as well, which can be interesting for further enhanced catalysis. Impregnation is less versatile and only a few adjustments can be made in the synthesis to alter, for example, the distribution of particles over the surface area.

Taking these considerations in mind, for further laboratory steps, electrodeposition seems the most sensible option to use for further trials towards a proof of concept of the slurry electrode, as it allows for study of more different types of catalysts and is easily scaled to a batch size large enough to produce one slurry. In future applications however, impregnation might be easier to implement.

### 5.2.2. Towards a proof of concept of the slurry electrode flow cell

The main problem in the execution of the catalysis experiments was the high potential on the anode side, most likely caused by oxygen bubbles. Solving this problem is not very straightforward, as it is a research topic on its own [66]. The simple alteration would be to change the geometry of the flow channel and/or the hydrophobicity of the anode, yet neither of these are a guaranteed solution and this problem has a tremendous effect on the cell's energy efficiency until an effective solution is found.

The other problem encountered in this thesis is an unexpected trend for the CO production by the slurry in the flow cell. To work towards an indisputable proof-of-concept of a reaction taking place on the slurry surface, it is recommended to first investigate the source of the current CO production. There are several different carbon sources present in the set-up, which can all have a contribution to the CO production and need to be investigated individually.

A reasonable next step would involve investigating the influence of the carbon paper current collector on the CO production. It is possible that the current collector is a part of the problem as a carbon source, nevertheless it cannot be the only source, since it does not explain the CO production differences between experiments, since they all had a fresh current collector of the same carbon paper source. To determine the influence of the carbon paper current collector, the catalysis experiment should be executed with electrolyte only, instead of a slurry. If CO is still measured among the products, then the carbon paper should be replaced with a more inert alternative. Even if this is not the case, replacement of the carbon current collector is also advised because of its poor physical stability.

The next step would be to study the influence of the carbon powder on the CO production. This is best done by creating a blank experiment with a bare powder that has undergone the same treatment as the coated powder, except without the silver precursor there. In this way, any residual superficial reactions occurring are now equally pre-treated from both samples. If the new blank is now producing (nearly) no CO and the silver coated sample produces more (and increasing with current density), there is a proof of concept. If this is not the case, more investigation on the CO production with bare carbon is necessary to suppress this reaction. Possible solutions could lie in an added surfactant to suppress self-reaction, removal of certain reagents (oxygen) or in a change of solvent.

# Bibliography

- [1] John Houghton. Global warming. *Reports on Progress in Physics*, 68(6):1343–1403, 2005. ISSN 0034-4885 1361-6633. doi: 10.1088/0034-4885/68/6/r02.
- [2] IPCC. Summary for policymakers. Report, IPCC, 2013.
- [3] IPCC. Climate change 2014: Synthesis report. contribution of working groups i, ii and iii to the fifth assessment report of the intergovernmental panel on climate change. Report, IPCC, 2014.
- [4] B. D. Santer, K. E. Taylor, T. M. L. Wigley, T. C. Johns, P. D. Jonesll, D. J. Karoly, J. F. B. Mitchell, A. H. Oort, J. E. Pennert, V. Ramaswamy, M. D. Schwarzkopf, R. J. Stouffer, and S. Tett. A search for human influences on the thermal structure of the atmosphere. *Nature*, 382:39–46, 1996. doi: <https://doi.org/10.1038/382039a0>.
- [5] John Cook, Dana Nuccitelli, Sarah A. Green, Mark Richardson, Bärbel Winkler, Rob Painting, Robert Way, Peter Jacobs, and Andrew Skuce. Quantifying the consensus on anthropogenic global warming in the scientific literature. *Environmental Research Letters*, 8(2), 2013. doi: 10.1088/1748-9326/8/2/024024.
- [6] John Cook, Naomi Oreskes, Peter T. Doran, William R. L. Anderegg, Bart Verheggen, Ed W. Maibach, J. Stuart Carlton, Stephan Lewandowsky, Andrew G. Skuce, Sarah A. Green, Dana Nuccitelli, Peter Jacobs, Mark Richardson, Bärbel Winkler, Rob Painting, and Ken Rice. Consensus on consensus: a synthesis of consensus estimates on human-caused global warming. *Environmental Research Letters*, 11(4), 2016. ISSN 1748-9326. doi: 10.1088/1748-9326/11/4/048002.
- [7] NASA Earth Observatory, 4-12-2007 2007. URL [https://www.nasa.gov/centers/langley/news/researchernews/rn\\_carboncycle.html](https://www.nasa.gov/centers/langley/news/researchernews/rn_carboncycle.html).
- [8] Rosa M. Cuéllar-Franca and Adisa Azapagic. Carbon capture, storage and utilisation technologies: A critical analysis and comparison of their life cycle environmental impacts. *Journal of CO2 Utilization*, 9:82–102, 2015. ISSN 22129820. doi: 10.1016/j.jcou.2014.12.001.
- [9] Edward J. Maginn. What to do with co2. *The Journal of Physical Chemistry Letters*, 1(24):3478–3479, 2010. ISSN 1948-7185. doi: 10.1021/jz101582c.
- [10] Peter Markewitz, Wilhelm Kuckshinrichs, Walter Leitner, Jochen Linssen, Petra Zapp, Richard Bongartz, Andrea Schreiber, and Thomas E. Müller. Worldwide innovations in the development of carbon capture technologies and the utilization of co2. *Energy & Environmental Science*, 5(6), 2012. ISSN 1754-5692 1754-5706. doi: 10.1039/c2ee03403d.
- [11] K. M. Yu, I. Curcic, J. Gabriel, and S. C. Tsang. Recent advances in co2 capture and utilization. *ChemSusChem*, 1(11):893–9, 2008. ISSN 1864-564X (Electronic) 1864-5631 (Linking). doi: 10.1002/cssc.200800169. URL <https://www.ncbi.nlm.nih.gov/pubmed/18985640>.
- [12] Gabriele Centi and Siglinda Perathoner. Opportunities and prospects in the chemical recycling of carbon dioxide to fuels. *Catalysis Today*, 148(3-4):191–205, 2009. ISSN 09205861. doi: 10.1016/j.cattod.2009.07.075.
- [13] Daan Jansen Peter Styring. Ccu in the green economy. Report, Centre for Low Carbon Futures, 2011.
- [14] Daniel P Schrag. Preparing to capture carbon. *Science*, 315(5813):812–813, 2007. doi: 10.1126/science.1137632.

- [15] G. A. Olah. Beyond oil and gas: the methanol economy. *Angew Chem Int Ed Engl*, 44(18):2636–9, 2005. ISSN 1433-7851 (Print) 1433-7851 (Linking). doi: 10.1002/anie.200462121. URL <https://www.ncbi.nlm.nih.gov/pubmed/15800867>.
- [16] Nils Thonemann and Massimo Pizzol. Consequential life cycle assessment of carbon capture and utilization technologies within the chemical industry. *Energy & Environmental Science*, 12(7):2253–2263, 2019. ISSN 1754-5692 1754-5706. doi: 10.1039/c9ee00914k.
- [17] D. M. Weekes, D. A. Salvatore, A. Reyes, A. Huang, and C. P. Berlinguette. Electrolytic co<sub>2</sub> reduction in a flow cell. *Acc Chem Res*, 51(4):910–918, 2018. ISSN 1520-4898 (Electronic) 0001-4842 (Linking). doi: 10.1021/acs.accounts.8b00010. URL <https://www.ncbi.nlm.nih.gov/pubmed/29569896>.
- [18] S. Verma, B. Kim, H. R. Jhong, S. Ma, and P. J. Kenis. A gross-margin model for defining technoeconomic benchmarks in the electroreduction of co<sub>2</sub>. *ChemSusChem*, 9(15):1972–9, 2016. ISSN 1864-564X (Electronic) 1864-5631 (Linking). doi: 10.1002/cssc.201600394. URL <https://www.ncbi.nlm.nih.gov/pubmed/27345560>.
- [19] Volker Presser, Christopher R. Dennison, Jonathan Campos, Kevin W. Knehr, Emin C. Kumbur, and Yury Gogotsi. The electrochemical flow capacitor: A new concept for rapid energy storage and recovery. *Advanced Energy Materials*, 2(7):895–902, 2012. ISSN 16146832. doi: 10.1002/aenm.201100768.
- [20] C. R. Dennison, M. Beidaghi, K. B. Hatzell, J. W. Campos, Y. Gogotsi, and E. C. Kumbur. Effects of flow cell design on charge percolation and storage in the carbon slurry electrodes of electrochemical flow capacitors. *Journal of Power Sources*, 247:489–496, 2014. ISSN 03787753. doi: 10.1016/j.jpowsour.2013.08.101.
- [21] Bilen Akuzum, Lutfi Agartan, J. Locco, and E. C. Kumbur. Effects of particle dispersion and slurry preparation protocol on electrochemical performance of capacitive flowable electrodes. *Journal of Applied Electrochemistry*, 47(3):369–380, 2017. ISSN 0021-891X 1572-8838. doi: 10.1007/s10800-017-1046-5.
- [22] Jonathan W. Campos, Majid Beidaghi, Kelsey B. Hatzell, Christopher R. Dennison, Benjamin Musci, Volker Presser, Emin C. Kumbur, and Yury Gogotsi. Investigation of carbon materials for use as a flowable electrode in electrochemical flow capacitors. *Electrochimica Acta*, 98:123–130, 2013. ISSN 00134686. doi: 10.1016/j.electacta.2013.03.037.
- [23] Ko Yeon Choo, Chung Yul Yoo, Moon Hee Han, and Dong Kook Kim. Electrochemical analysis of slurry electrodes for flow-electrode capacitive deionization. *Journal of Electroanalytical Chemistry*, 806:50–60, 2017. ISSN 15726657. doi: 10.1016/j.jelechem.2017.10.040.
- [24] Johannes Lohaus, Deniz Rall, Maximilian Kruse, Viktoria Steinberger, and Matthias Wessling. On charge percolation in slurry electrodes used in vanadium redox flow batteries. *Electrochemistry Communications*, 101:104–108, 2019. ISSN 13882481. doi: 10.1016/j.elecom.2019.02.013.
- [25] Nathalie E.G. Ligthart. Conductivity of suspension electrodes. Presented during group meeting, 14-01-2021.
- [26] R. Kortlever, J. Shen, K. J. Schouten, F. Calle-Vallejo, and M. T. Koper. Catalysts and reaction pathways for the electrochemical reduction of carbon dioxide. *J Phys Chem Lett*, 6(20):4073–82, 2015. ISSN 1948-7185 (Electronic) 1948-7185 (Linking). doi: 10.1021/acs.jpcllett.5b01559. URL <https://www.ncbi.nlm.nih.gov/pubmed/26722779>.
- [27] R. Sharifian, R. M. Wagterveld, I. A. Digdaya, C. Xiang, and D. A. Vermaas. Electrochemical carbon dioxide capture to close the carbon cycle. *Energy & Environmental Science*, 14(2):781–814, 2021. ISSN 1754-5692 1754-5706. doi: 10.1039/d0ee03382k.
- [28] John-Paul Jones, G. K. Surya Prakash, and George A. Olah. Electrochemical co<sub>2</sub> reduction: Recent advances and current trends. *Israel Journal of Chemistry*, 54(10):1451–1466, 2014. ISSN 00212148. doi: 10.1002/ijch.201400081.

- [29] Yoshio Hori, Hidetoshi Wakabe, Toshio Tsukamoto, and Osamu Koga. Electrocatalytic process of co selectivity in electrochemical reduction of co<sub>2</sub> at metal electrodes in aqueous media. *Electrochimica Acta*, 39(11/12):1833–1839, 1994. doi: [https://doi.org/10.1016/0013-4686\(94\)85172-7](https://doi.org/10.1016/0013-4686(94)85172-7).
- [30] Y. Hori. *Electrochemical CO<sub>2</sub> Reduction on Metal Electrodes*, pages 89–189. Springer New York, New York, NY, 2008. ISBN 978-0-387-49489-0. doi: 10.1007/978-0-387-49489-0\_3. URL [https://doi.org/10.1007/978-0-387-49489-0\\_3](https://doi.org/10.1007/978-0-387-49489-0_3).
- [31] R. Becker and W. Döring. Kinetische behandlung der keimbildung in übersättigten dämpfen. *Annalen der Physik*, 416(8):719–752, 1935. ISSN 0003-3804. doi: <https://doi.org/10.1002/andp.19354160806>. URL <https://onlinelibrary.wiley.com/doi/abs/10.1002/andp.19354160806>.
- [32] V. K. La Mer. Nucleation in phase transitions. *Industrial and Engineering Chemistry*, 44(6):1270–1277, 1952. doi: <https://doi.org/10.1021/ie50510a027>.
- [33] Jörg Polte. Fundamental growth principles of colloidal metal nanoparticles – a new perspective. *CrystEngComm*, 17(36):6809–6830, 2015. ISSN 1466-8033. doi: 10.1039/c5ce01014d.
- [34] Victor K. LaMer and Robert H. Dinegar. Theory, production and mechanism of formation of monodispersed hydrosols. *Journal of the American Chemical Society*, 72(11):4847–4854, 1950. ISSN 0002-7863. doi: 10.1021/ja01167a001. URL <https://doi.org/10.1021/ja01167a001>.
- [35] Amin Salehi-Khojin, Huei-Ru Molly Jhong, Brian A. Rosen, Wei Zhu, Sichao Ma, Paul J. A. Kenis, and Richard I. Masel. Nanoparticle silver catalysts that show enhanced activity for carbon dioxide electrolysis. *The Journal of Physical Chemistry C*, 117(4):1627–1632, 2013. ISSN 1932-7447 1932-7455. doi: 10.1021/jp310509z. URL <https://pubs.acs.org/doi/pdf/10.1021/jp310509z>.
- [36] Seoin Back, Min Sun Yeom, and Yousung Jung. Active sites of au and ag nanoparticle catalysts for co<sub>2</sub> electroreduction to co. *ACS Catalysis*, 5(9):5089–5096, 2015. ISSN 2155-5435 2155-5435. doi: 10.1021/acscatal.5b00462.
- [37] Samah A. Mahyoub, Fahim A. Qaraah, Chengzhen Chen, Fanghua Zhang, Shenglin Yan, and Zhenmin Cheng. An overview on the recent developments of ag-based electrodes in the electrochemical reduction of co<sub>2</sub> to co. *Sustainable Energy & Fuels*, 4(1):50–67, 2020. ISSN 2398-4902. doi: 10.1039/c9se00594c.
- [38] C. Kim, H. S. Jeon, T. Eom, M. S. Jee, H. Kim, C. M. Friend, B. K. Min, and Y. J. Hwang. Achieving selective and efficient electrocatalytic activity for co<sub>2</sub> reduction using immobilized silver nanoparticles. *J Am Chem Soc*, 137(43):13844–50, 2015. ISSN 1520-5126 (Electronic) 0002-7863 (Linking). doi: 10.1021/jacs.5b06568. URL <https://www.ncbi.nlm.nih.gov/pubmed/26447349>.
- [39] J. Park, J. Joo, S. G. Kwon, Y. Jang, and T. Hyeon. Synthesis of monodisperse spherical nanocrystals. *Angew Chem Int Ed Engl*, 46(25):4630–60, 2007. ISSN 1433-7851 (Print) 1433-7851 (Linking). doi: 10.1002/anie.200603148. URL <https://www.ncbi.nlm.nih.gov/pubmed/17525914>.
- [40] Jie Ding, Yunfei Bu, Man Ou, Yang Yu, Qin Zhong, and Maohong Fan. Facile decoration of carbon fibers with ag nanoparticles for adsorption and photocatalytic reduction of co<sub>2</sub>. *Applied Catalysis B: Environmental*, 202:314–325, 2017. ISSN 09263373. doi: 10.1016/j.apcatb.2016.09.038.
- [41] Zongtao Zhang, Bin Zhao, and Liming Hu. Pvp protective mechanism of ultrafine silver powder synthesized by chemical reduction processes. *Journal of Solid State Chemistry*, 121(1):105–110, 1996. doi: <https://doi.org/10.1006/jssc.1996.0015>.
- [42] Sally D. Solomon, Mozghan Bahadory, Aravindan V. Jeyarajasingam, Susan A. Rutkowsky, and Charles Boritz. Synthesis and study of silver nanoparticles. *Journal of Chemical Education*, 84(2):322–325, 2007. doi: <https://doi.org/10.1021/ed084p322>.

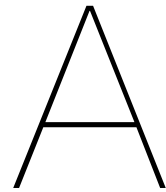
- [43] Emanuela Filippo, Antonio Serra, Alessandro Buccolieri, and Daniela Manno. Green synthesis of silver nanoparticles with sucrose and maltose: Morphological and structural characterization. *Journal of Non-Crystalline Solids*, 356(6-8):344–350, 2010. ISSN 00223093. doi: 10.1016/j.jnoncrysol.2009.11.021.
- [44] Yu Seok Ham, Seunghoe Choe, Myung Jun Kim, Taeho Lim, Soo-Kil Kim, and Jae Jeong Kim. Electrodeposited ag catalysts for the electrochemical reduction of co 2 to co. *Applied Catalysis B: Environmental*, 208:35–43, 2017. ISSN 09263373. doi: 10.1016/j.apcatb.2017.02.040.
- [45] J. Ruud van Ommen, Caner U. Yurteri, Naoko Ellis, and Erik M. Kelder. Scalable gas-phase processes to create nanostructured particles. *Particuology*, 8(6):572–577, 2010. ISSN 16742001. doi: 10.1016/j.partic.2010.07.010.
- [46] P. Munnik, P. E. de Jongh, and K. P. de Jong. Recent developments in the synthesis of supported catalysts. *Chem Rev*, 115(14):6687–718, 2015. ISSN 1520-6890 (Electronic) 0009-2665 (Linking). doi: 10.1021/cr500486u. URL <https://www.ncbi.nlm.nih.gov/pubmed/26088402>.
- [47] Peter Munnik, Nynke A. Krans, Petra E. de Jongh, and Krijn P. de Jong. Effects of drying conditions on the synthesis of co/sio2 and co/al2o3 fischer–tropsch catalysts. *ACS Catalysis*, 4(9):3219–3226, 2014. ISSN 2155-5435 2155-5435. doi: 10.1021/cs5006772.
- [48] Tamara M. Eggenhuisen, Heiner Friedrich, Fabio Nudelman, Jovana Zečević, Nico A. J. M. Sommerdijk, Petra E. de Jongh, and Krijn P. de Jong. Controlling the distribution of supported nanoparticles by aqueous synthesis. *Chemistry of Materials*, 25(6):890–896, 2013. ISSN 0897-4756 1520-5002. doi: 10.1021/cm3037845.
- [49] H. Van Bui, F. Grillo, and J. R. van Ommen. Atomic and molecular layer deposition: off the beaten track. *Chem Commun (Camb)*, 53(1):45–71, 2016. ISSN 1364-548X (Electronic) 1359-7345 (Linking). doi: 10.1039/c6cc05568k. URL <https://www.ncbi.nlm.nih.gov/pubmed/27725977>.
- [50] Ville Miikkulainen, Markku Leskelä, Mikko Ritala, and Riikka L. Puurunen. Crystallinity of inorganic films grown by atomic layer deposition: Overview and general trends. *Journal of Applied Physics*, 113(2), 2013. ISSN 0021-8979 1089-7550. doi: 10.1063/1.4757907.
- [51] A. Niskanen, T. Hatanpää, K. Arstila, M. Leskelä, and M. Ritala. Radical-enhanced atomic layer deposition of silver thin films using phosphine-adducted silver carboxylates. *Chemical Vapor Deposition*, 13(8):408–413, 2007. ISSN 09481907 15213862. doi: 10.1002/cvde.200606519.
- [52] P. R. Chalker, S. Romani, P. A. Marshall, M. J. Rosseinsky, S. Rushworth, and P. A. Williams. Liquid injection atomic layer deposition of silver nanoparticles. *Nanotechnology*, 21(40):405602, 2010. ISSN 1361-6528 (Electronic) 0957-4484 (Linking). doi: 10.1088/0957-4484/21/40/405602. URL <https://www.ncbi.nlm.nih.gov/pubmed/20829564>.
- [53] Wikipedia, 2021. URL [https://en.wikipedia.org/wiki/Transmission\\_electron\\_microscopy](https://en.wikipedia.org/wiki/Transmission_electron_microscopy).
- [54] William D. Pyrz and Douglas J. Buttrey. Particle size determination using tem: A discussion of image acquisition and analysis for the novice microscopist. *Langmuir*, 24(20):11350–11360, 2008. ISSN 0743-7463. doi: 10.1021/la801367j. URL <https://doi.org/10.1021/la801367j>.
- [55] Wiskunde en Informatica Radboud Universiteit, Faculteit der Natuurwetenschappen, 2021. URL <https://www.ru.nl/fnwi/gi/faciliteiten-activiteiten/element-analyse/icp-oes/>.
- [56] Mindy Levine, 2020. URL <https://www.technologynetworks.com/analysis/articles/icp-oes-icp-chemistry-icp-oes-analysis-strengths-and-limitations-342265>.
- [57] ChemViews Magazine, 2017. URL [https://www.chemistryviews.org/details/ezone/10463356/X-Ray\\_Photoelectron\\_Spectroscopy\\_XPS.html](https://www.chemistryviews.org/details/ezone/10463356/X-Ray_Photoelectron_Spectroscopy_XPS.html).

- [58] Wikipedia, 2021. URL [https://en.wikipedia.org/wiki/X-ray\\_photoelectron\\_spectroscopy](https://en.wikipedia.org/wiki/X-ray_photoelectron_spectroscopy).
- [59] Thermo Fisher Scientific, 2021. URL <https://xpssimplified.com/whatisxps.php>.
- [60] Wikipedia, 2021. URL [https://en.wikipedia.org/wiki/Gas\\_chromatography](https://en.wikipedia.org/wiki/Gas_chromatography).
- [61] Faculteit Civiele Techniek en Geowetenschappen Technische Universiteit Delft, 2021. URL <https://www.tudelft.nl/citg/over-faculteit/afdelingen/watermanagement/research/waterlab/equipment/gas-chromatography-gc>.
- [62] Harold M. McNair, James M. Miller, and Nicholas H. Snow. *BASIC CONCEPTS AND TERMS*, pages 15–35. Wiley, 2019. doi: <https://doi.org/10.1002/9781119450795.ch2>. URL <https://onlinelibrary.wiley.com/doi/abs/10.1002/9781119450795.ch2>.
- [63] Q. Hong and H. Lu. In-situ electrodeposition of highly active silver catalyst on carbon fiber papers as binder free cathodes for aluminum-air battery. *Sci Rep*, 7(1):3378, 2017. ISSN 2045-2322 (Electronic) 2045-2322 (Linking). doi: 10.1038/s41598-017-03609-9. URL <https://www.ncbi.nlm.nih.gov/pubmed/28611456>.
- [64] P. H. Keijzer, B. Donoeva, K. P. de Jong, and P. E. de Jongh. Supported silver catalysts prepared via melt infiltration: Synthesis, characterization and performance in selective hydrogenation. *Catalysis Today*, 2020. ISSN 09205861. doi: 10.1016/j.cattod.2020.03.017.
- [65] M. H. Miles and M. A. Thomason. Periodic variations of overvoltages for water electrolysis in acid solutions from cyclic voltammetry studies. *Journal of The Electrochemical Society*, 123(10): 1459–1461, 1976. doi: <https://doi.org/10.1149/1.2132619>.
- [66] Andrea Angulo, Peter van der Linde, Han Gardeniers, Miguel Modestino, and David Fernández Rivas. Influence of bubbles on the energy conversion efficiency of electrochemical reactors. *Joule*, 4(3):555–579, 2020. ISSN 25424351. doi: 10.1016/j.joule.2020.01.005.



# Appendices





## Additional deposition data

### A.1. Silver oxidation state

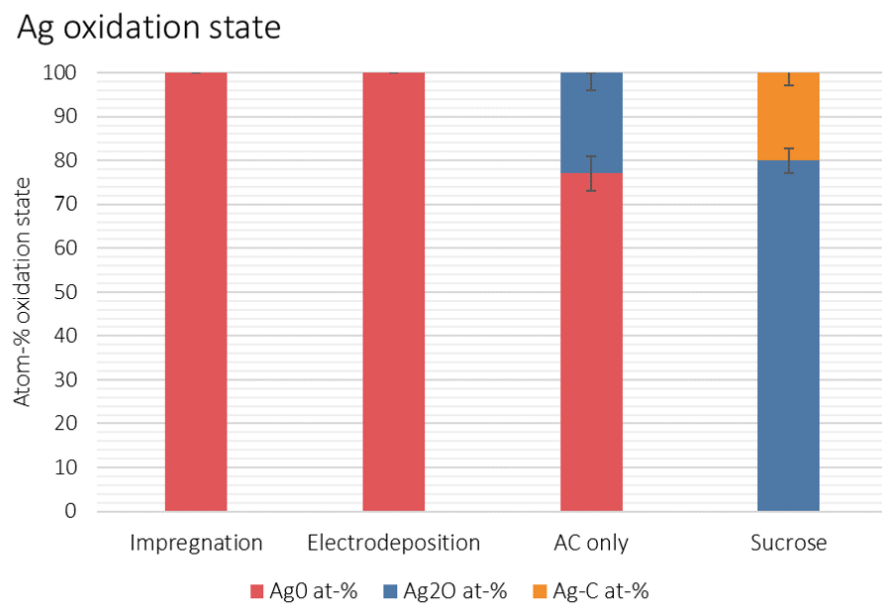


Figure A.1: Silver oxidation states in atomic percentages per synthesis method, measured after deposition of silver.

## A.2. Particle size distribution

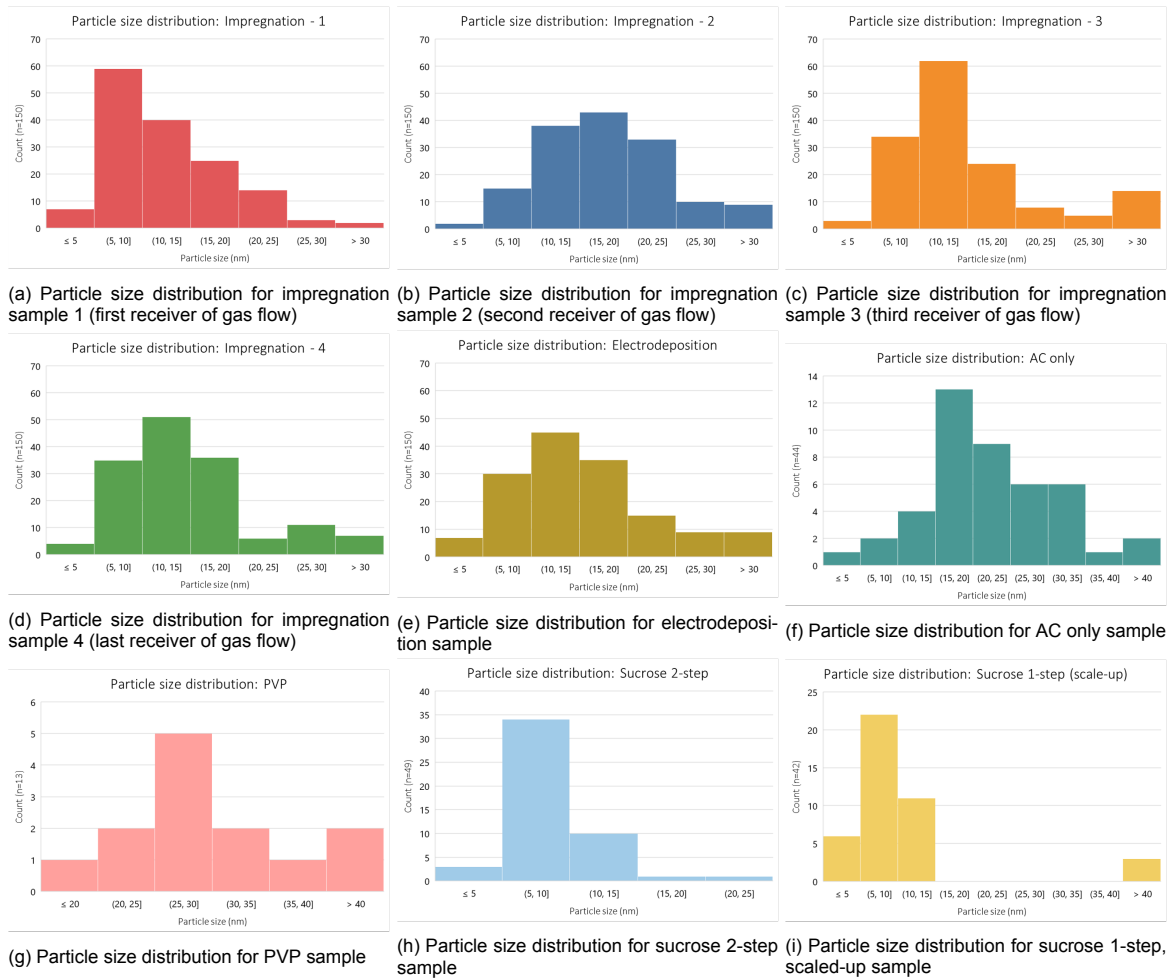
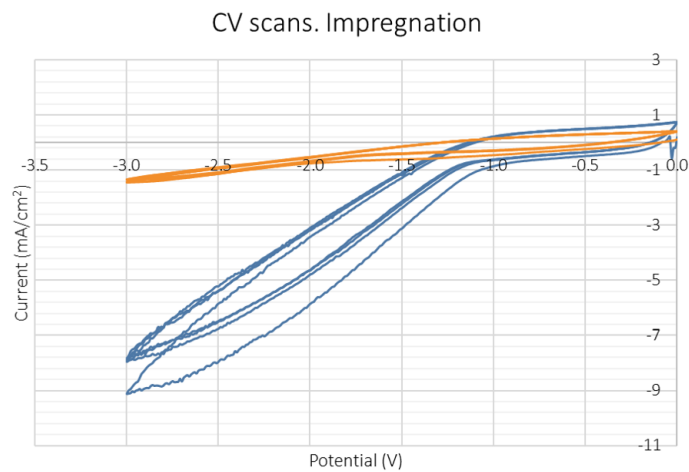


Figure A.2: Particle size distribution per sample. Count 150 or lower (when only fewer particles could be measured). Bin size 5 nm, with overflow below 5 nm and above 40 nm. A higher lowest bin means that any lower bins were empty (e.g. <10 nm shows the count for 5-10 nm and lower bins were empty). A lower highest bin means that no particles were observed above that bin (e.g. >30 nm shows the count for 30-35 nm and higher bins were empty).

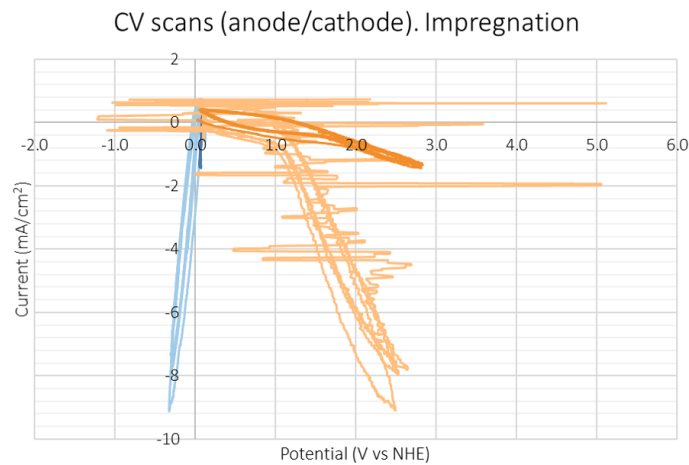
# B

## Additional electrochemical data

### B.1. Impregnation

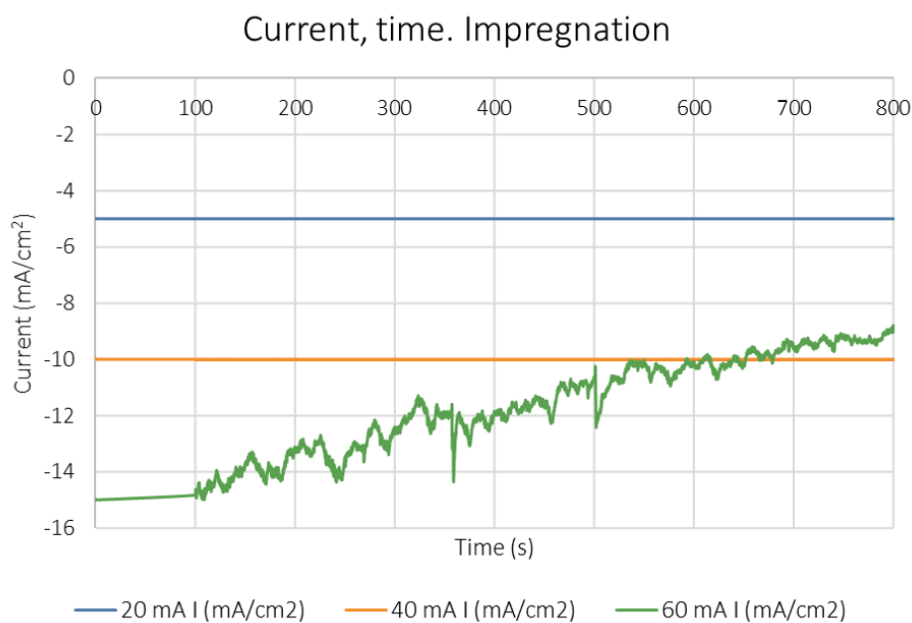


(a) CV scans, WE potential before (blue) and after (orange) catalysis experiment.

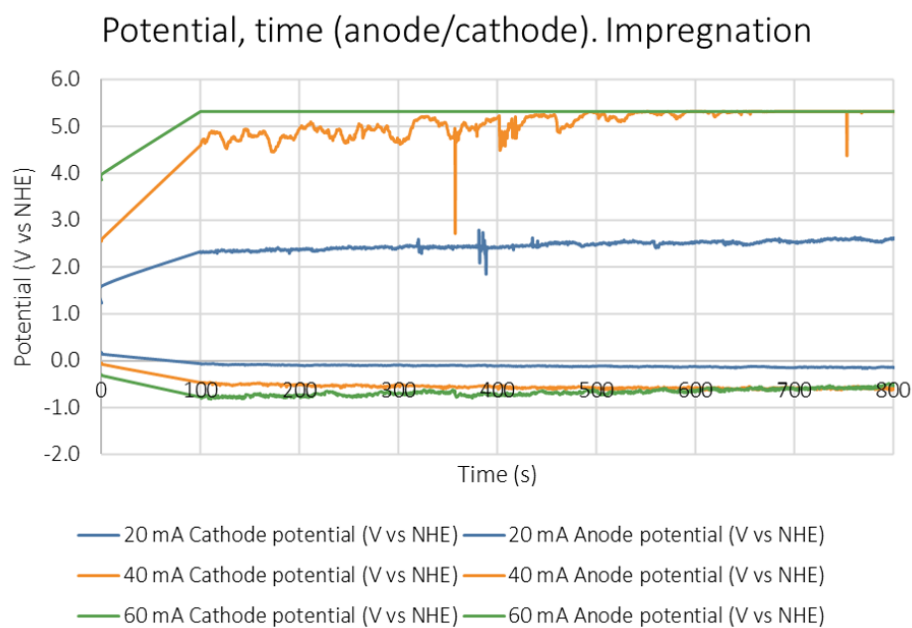


(b) CV scans, anodic (orange) and cathodic (blue) potentials, measured before (light) and after (dark) the catalysis experiment.

Figure B.1: CV scans before and after catalysis experiment with impregnation sample, four cycles, measured from 0 V to -3 V at scan rate 100 mV/s.

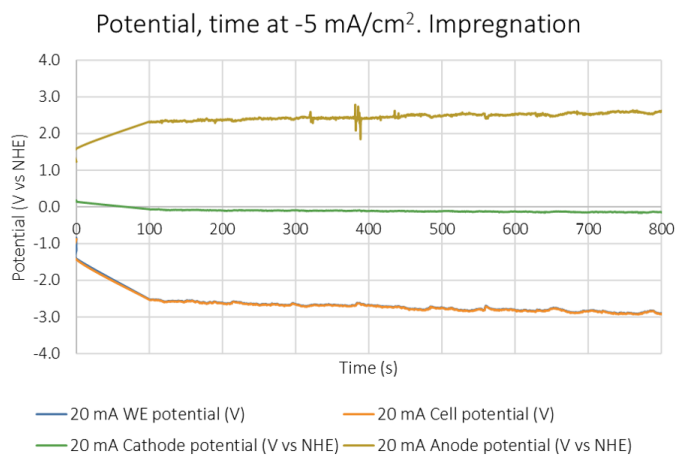


(a) Combined current over time measurements from the catalysis experiments with the impregnation sample.

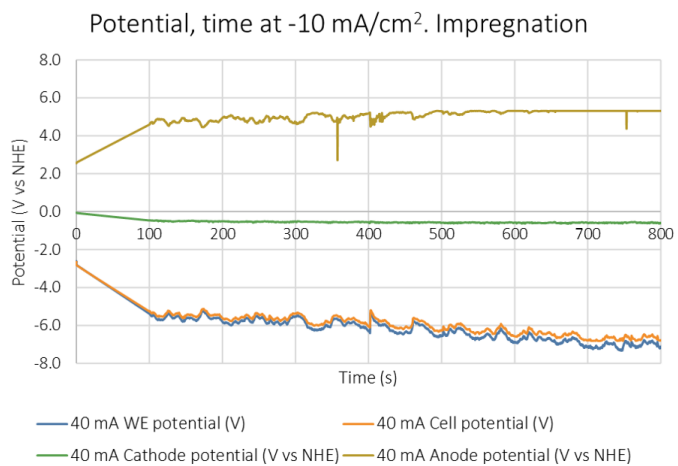


(b) Combined potential over time measurements from the catalysis experiments with the impregnation sample. Anodic potentials (positive) increase more than two-fold within the measured current range to 5 V versus NHE. Cathodic potentials (negative) barely increase with increasing current density. Color represents experiment.

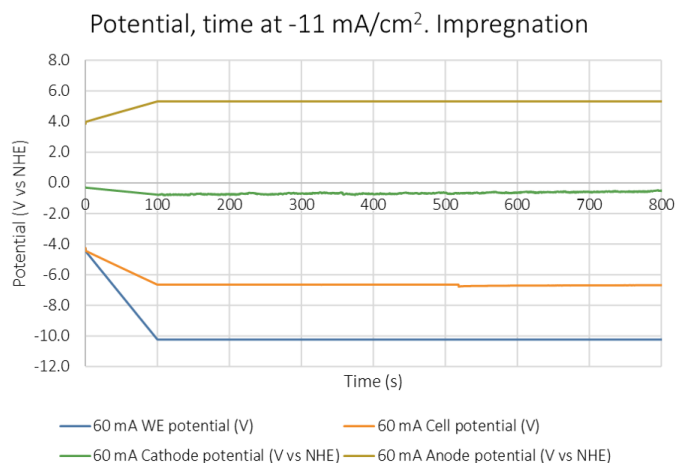
Figure B.2: Current and potential over time measurements from catalysis experiments with the impregnation sample.



(a) Potential over time measurements during catalysis experiment at -5 mA/cm<sup>2</sup>.



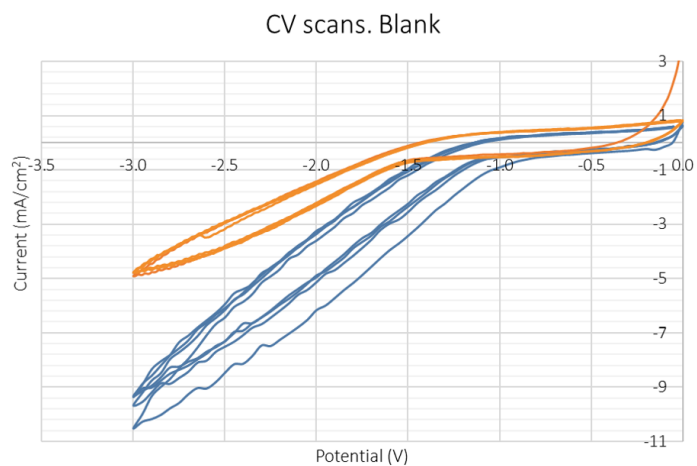
(b) Potential over time measurements during catalysis experiment with impregnation sample at -10 mA/cm<sup>2</sup>.



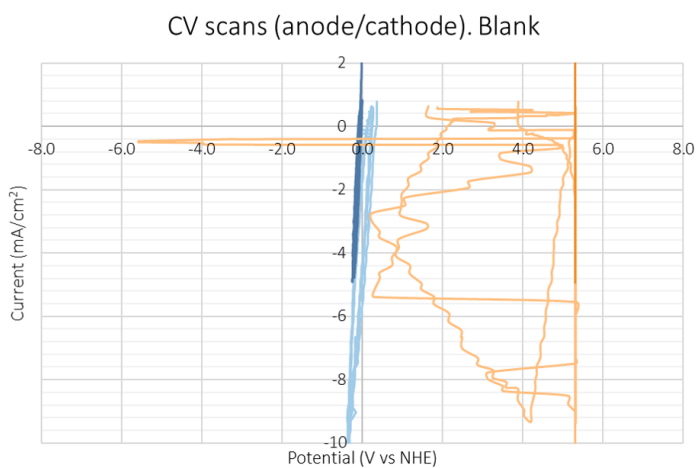
(c) Potential over time measurements during catalysis experiment at -11 mA/cm<sup>2</sup>.

Figure B.3: WE, cell, cathode, anode potential over time measurements from catalysis experiment with impregnation sample.

## B.2. Blank

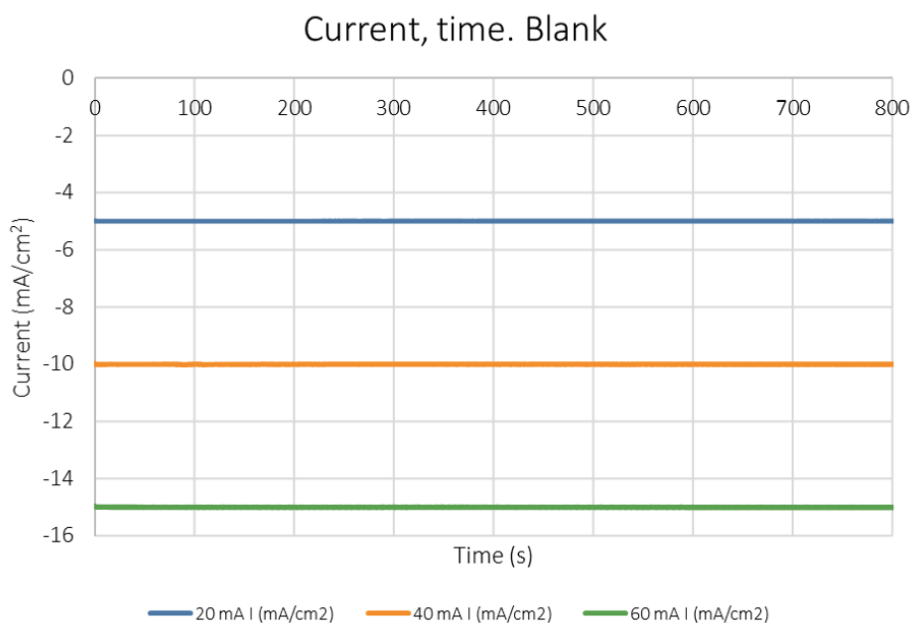


(a) CV scans, WE potential before (blue) and after (orange) catalysis experiment.

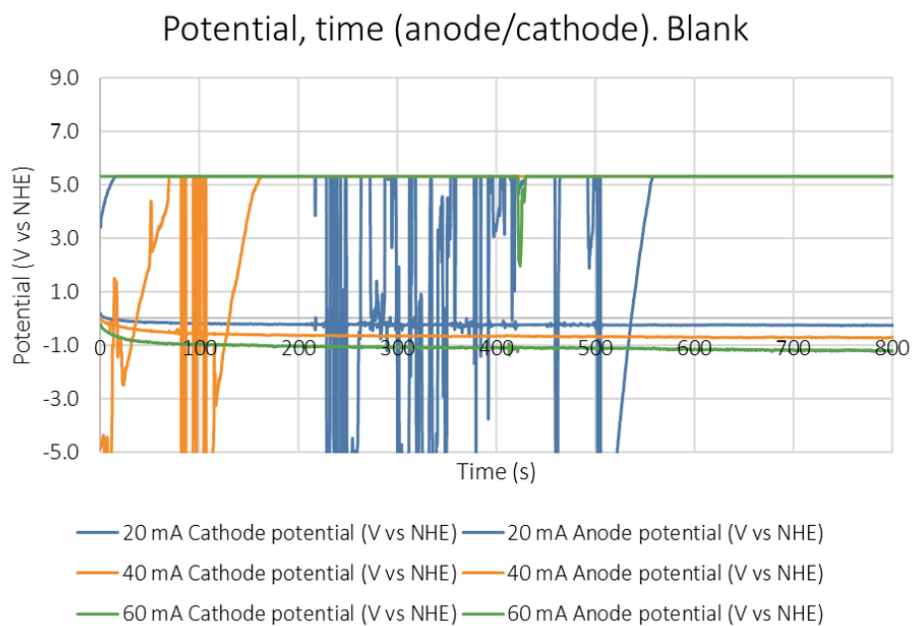


(b) CV scans, anodic (orange) and cathodic (blue) potentials, measured before (light) and after (dark) the catalysis experiment.

Figure B.4: CV scans before and after catalysis experiment with blank sample, four cycles, measured from 0 V to -3 V at scan rate 100 mV/s.



(a) Combined current over time measurements from the catalysis experiments with the blank sample.



(b) Combined potential over time measurements from the catalysis experiments with the blank sample. Anodic potentials (positive) show a lot of noise/irregularities and are mostly at 5 V versus NHE. Cathodic potentials (negative) barely increase with increasing current density. Color represents current density of experiment.

Figure B.5: Current and potential over time measurements from catalysis experiments with the blank sample.

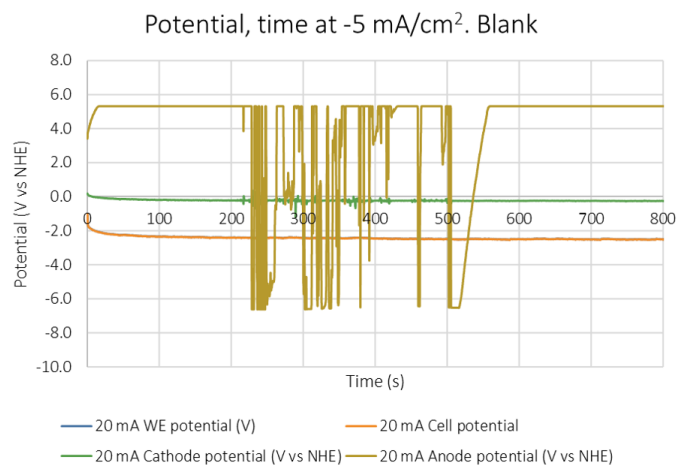
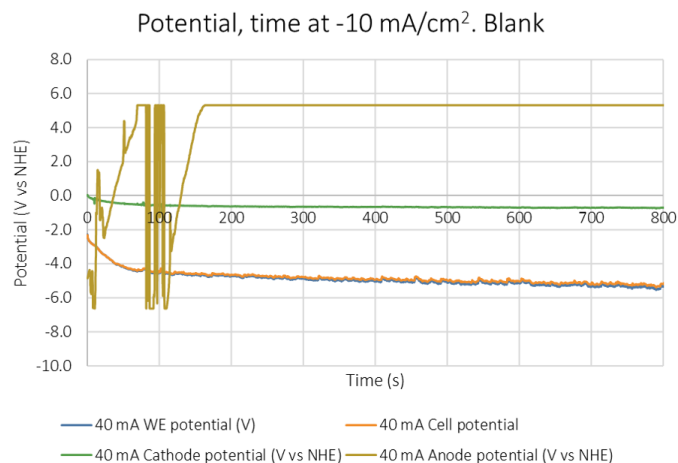
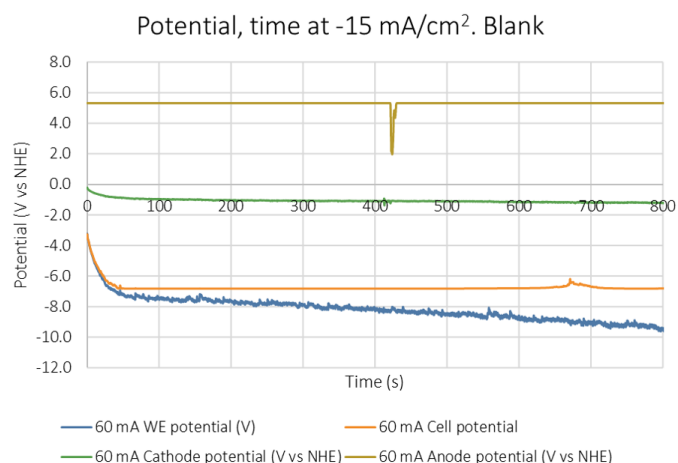
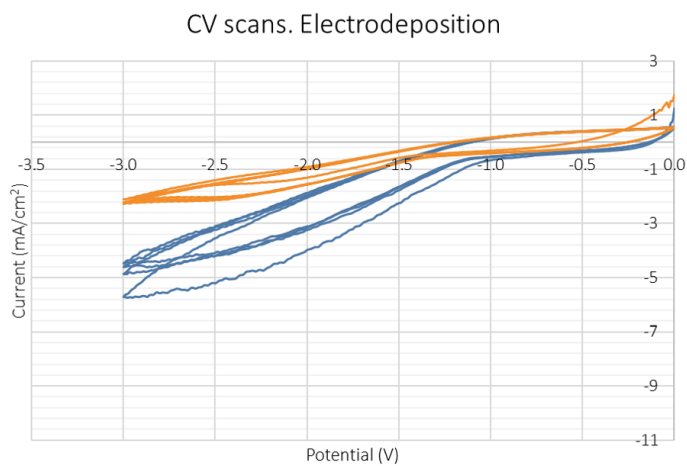
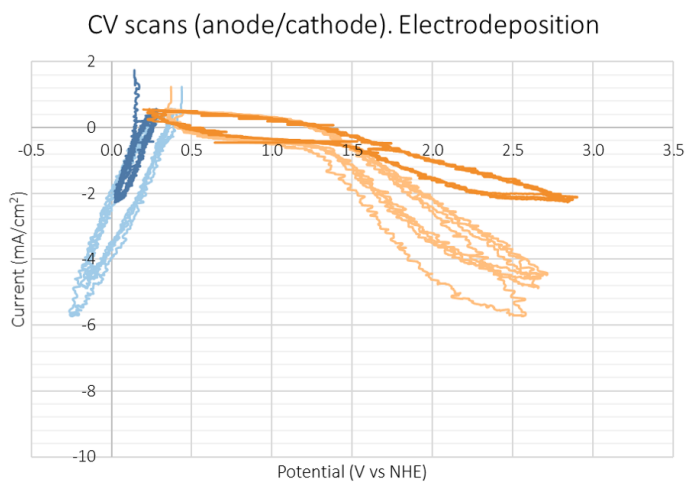
(a) Potential over time measurements during catalysis experiment at  $-5 \text{ mA/cm}^2$ .(b) Potential over time measurements during catalysis experiment with blank sample at  $-10 \text{ mA/cm}^2$ .(c) Potential over time measurements during catalysis experiment at  $-15 \text{ mA/cm}^2$ .

Figure B.6: WE, cell, cathode, anode potential over time measurements from catalysis experiment with blank sample.

## B.3. Electrodeposition

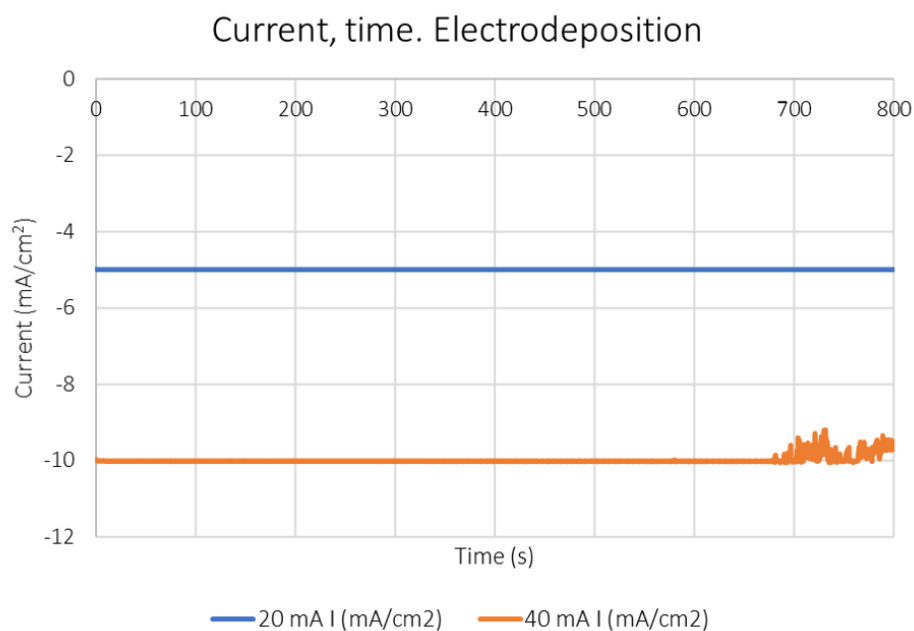


(a) CV scans, WE potential before (blue) and after (orange) catalysis experiment.

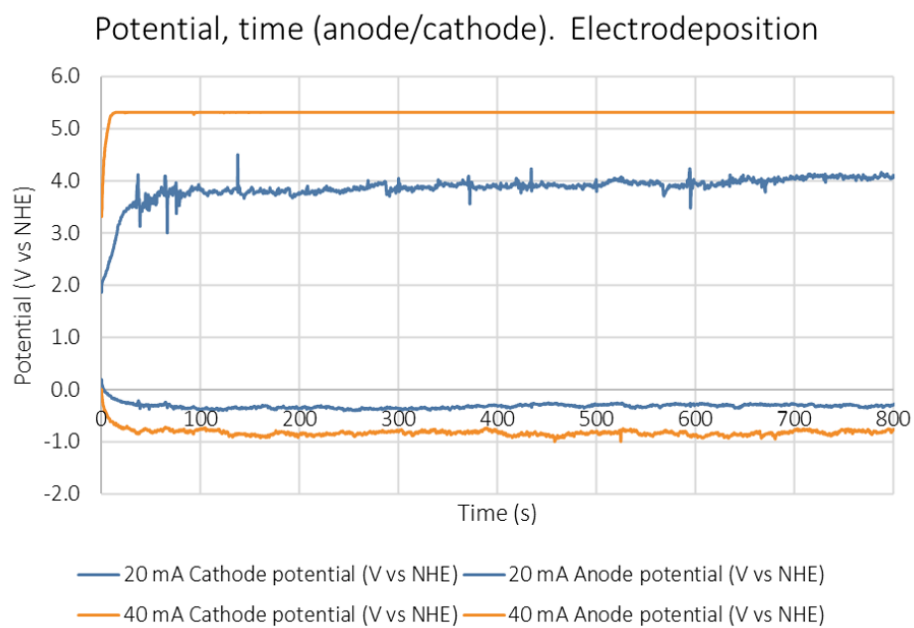


(b) CV scans, anodic (orange) and cathodic (blue) potentials, measured before (light) and after (dark) the catalysis experiment.

Figure B.7: CV scans before and after catalysis experiment with electrodeposition sample, four cycles, measured from 0 V to -3 V at scan rate 100 mV/s.

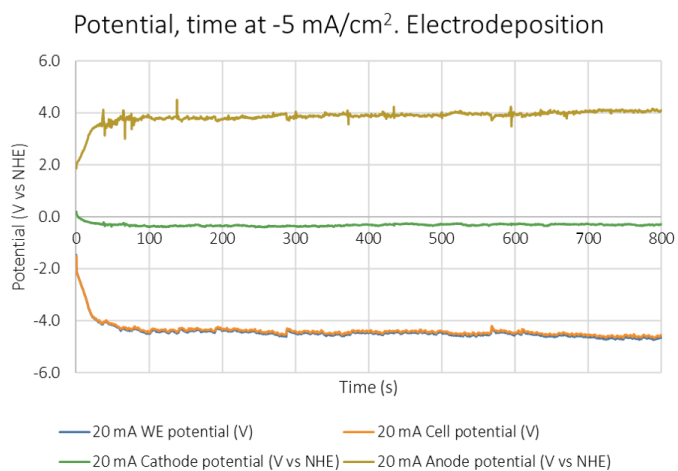


(a) Combined current over time measurements from the catalysis experiments with the electrodeposition sample.

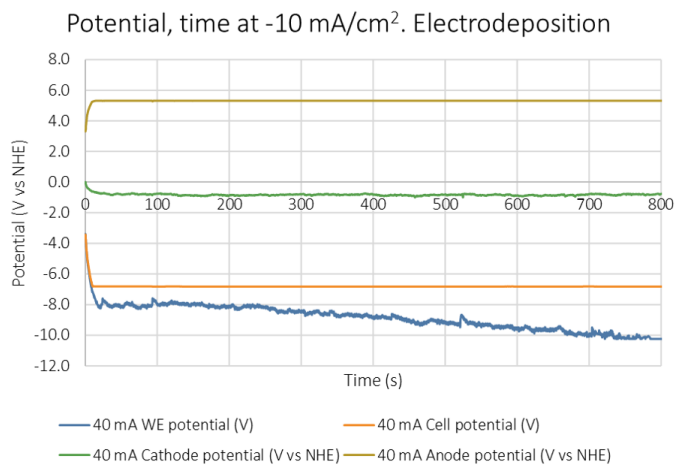


(b) Combined potential over time measurements from the catalysis experiments with the electrodeposition sample. Anodic potentials (positive) show a lot of noise/irregularities and are mostly at 5 V versus NHE. Cathodic potentials (negative) barely increase with increasing current density. Color represents current density of experiment.

Figure B.8: Current and potential over time measurements from catalysis experiments with the electrodeposition sample.



(a) Potential over time measurements during catalysis experiment at -5 mA/cm<sup>2</sup>.



(b) Potential over time measurements during catalysis experiment with electrodeposition sample at -10 mA/cm<sup>2</sup>.

Figure B.9: WE, cell, cathode, anode potential over time measurements from catalysis experiment with electrodeposition sample.

## B.4. CO<sub>2</sub> flow rate

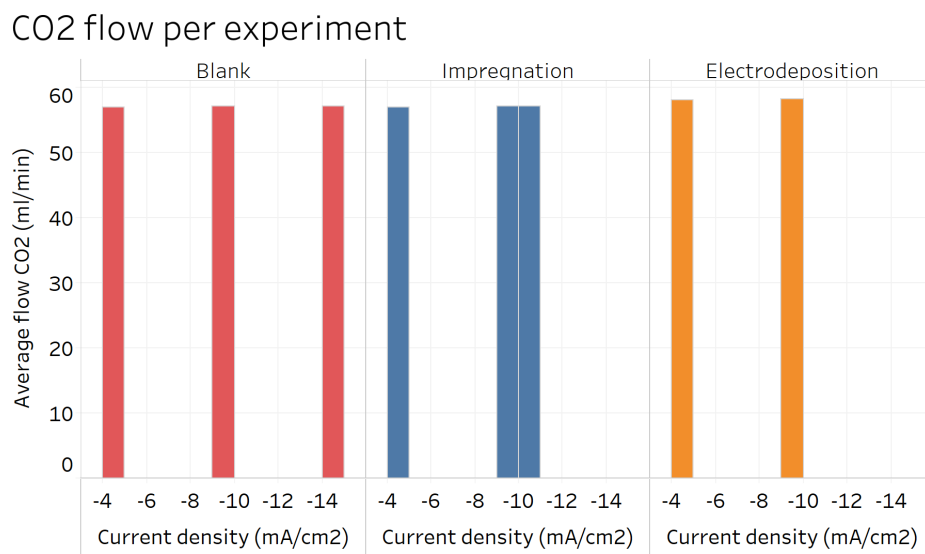


Figure B.10: CO<sub>2</sub> flow rate at current density, per sample.